USGS Award G16AP00014

Validation of a Geospatial Liquefaction Model for Noncoastal Regions Including Nepal

Laurie G. Baise and Vahid Rashidian
Department of Civil and Environmental Engineering
Tufts University
200 College Ave
Medford, MA 02155
617-627-2211
617-627-2994
laurie.baise@tufts.edu

March 2016 – September 2017

Validation of a Geospatial Liquefaction Model for Noncoastal Regions Including Nepal

Laurie G. Baise and Vahid Rashidian

Civil and Environmental Engineering Department, Tufts University, Medford, MA. 02155

1. Abstract

Soil liquefaction can lead to significant infrastructure damage after an earthquake due to lateral ground movements and vertical settlements. Regional liquefaction hazard maps are important in both planning for earthquake events and guiding relief efforts. New liquefaction hazard mapping techniques based on readily available geospatial data allow for an integration of liquefaction hazard in loss estimation platforms such as USGS's PAGER system. The global geospatial liquefaction model (GGLM) proposed by Zhu et al. (2017) and recommended for global application results in a liquefaction probability that can be interpreted as liquefaction spatial extent (LSE). The model uses ShakeMap's PGV, topography-based Vs_{30}, distance to coast, distance to river and annual precipitation as explanatory variables. This model has been tested previously with a focus on coastal settings. In this paper, LSE maps have been generated for more than 50 earthquakes around the world in a wide range of setting to evaluate the generality and regional efficacy of the model. The model performance is evaluated through comparisons with field observation reports of liquefaction. In addition, an intensity score for easy reporting and comparison is generated for each earthquake through the summation of LSE values and compared with the liquefaction intensity inferred from the reconnaissance report. The intensity scores are reported as an index for easy interpretation and reporting.

2. Introduction

Loosely deposited, cohesionless, and saturated soils may liquefy during cyclic loading from a major earthquake. Liquefaction may in turn induce ground failures of varying severity and result in damage to the built environment. Soil vulnerability to liquefaction depends on density (geotechnical properties of soil), water table depth (saturation) and earthquake demand (dynamic load). These factors are known to be dependent on geological age, depositional environment, topography, distance to water body and regional seismicity. Liquefaction assessment is an important component of an earthquake risk and loss evaluation for use in pre and post event planning and mitigation. Zhu et al. (2015, 2017) developed a globally-applicable geospatial liquefaction model that predicts probability and spatial extent of liquefaction for use in developing liquefaction hazard maps for use in rapid response and loss estimation.

The Zhu et al. (2015, 2017) geospatial liquefaction model (GLM) uses globally available geospatial explanatory variables that are proxies for density, saturation and dynamic loading. The Zhu et al. (2015) publication used four earthquakes from New Zealand and Japan in which liquefaction observations were spatially complete across each region (both liquefaction and non-liquefaction were mapped as continuous polygons). The model was developed using logistic regression. In Zhu et al. (2017), the GLM was updated by adding 23 earthquakes from China, Taiwan, Japan and the United States; however, the additional earthquakes were not mapped spatially complete, instead liquefaction and non-liquefaction occurrences were mostly point data. The Zhu et al. (2017) publication proposed two alternate GLMs: one for coastal earthquakes (according to Zhu et al. (2017): “events where the liquefaction occurrences are, on average, within 20 km of the coast; or, for earthquakes with insignificant or no liquefaction, epicentral distances less than 50 km”) and one for non-coastal earthquakes. Eighteen geospatial features were

compared as proxies for density, saturation and dynamic loading of earthquake. The coastal GLM used PGV, Vs_{30}, distance to coast, distance to river and precipitation as the explanatory variables. The global (or non-coastal) GLM used PGV, Vs_{30}, distance to water body (defined as minimum of distance to coast and distance to river), ground water table depth and precipitation as the explanatory variables. The Zhu et al. (2017) publication also proposed a logistic function to translate the GLM liquefaction probability to an estimate of the spatial extent of liquefaction. This allows the resulting map to provide an estimate of the fractional area of liquefaction within a pixel/polygon.

Liquefaction hazard mapping techniques that are based on readily available geospatial data such as developed by Zhu et. al (2015, 2017) allow for an integration of liquefaction hazard in loss estimation platforms such as U.S. Geological Survey's Prompt Assessment of Global Earthquakes for Response (PAGER) system (Wald et al., 2010). Quantifying earthquake secondary hazard impacts such as earthquake-induced liquefaction and estimating losses demand the development of a liquefaction impact scale that can be easily reported and integrated into a loss estimation system such as the PAGER system. To this end, this study has tested the global geospatial liquefaction model (GGLM) proposed by Zhu et.al (2017) across 54 earthquakes to evaluate model performance and to enhance the integration into a loss estimation system such as PAGER. The GGLM takes the USGS ShakeMap as a primary base layer and estimates the probability and spatial extent of liquefaction. In this study, we have modified the GGLM threshold in order to improve its performance. The GGLM performance has been evaluated and validated using observed liquefaction reported by reconnaissance teams after each individual event. Once the model performance is satisfactory, the liquefaction spatial extent (LSE) is summed for each earthquake. The goal of this work is to create a liquefaction intensity scale that is based on the GGLM-

estimated LSE. All 54 reconnaissance reports have been carefully evaluated and earthquakes are classified into 4 liquefaction intensity categories. The GGLM-based LSE values are then compared with the liquefaction intensity classification derived from field observation reports to derive an appropriate liquefaction intensity scale.

3. Database and Methodology

Zhu et al. (2017) presented two geospatial models for predicting liquefaction probability. While the coastal model relies on the distance to coast as a proxy for saturation and soil density, the global model uses distance to water and water table depth as the saturation proxies. As a result, the global model is recommended for global implementation and is preferred by the USGS (Thompson, personal communication, 2017) whereas the coastal model might be recommended for a regional implementation in a coastal environment. Both models were developed using logistic regression. The global geospatial liquefaction model (GGLM) used herein is described by the following equations:

$$P(x) = \begin{cases} \dfrac{1}{1+e^{-X}} & \text{If PGV > 3 cm/s AND Vs30 < 620 m/s} \\ 0 & \text{Otherwise} \end{cases} \quad (1)$$

P(x) is the probability of liquefaction which lies between zero and 1; and X includes explanatory variables that describes density, saturation and loading conditions and is given by:

$$X = 8.801 + a_1.ln(PGV) + a_2.ln(Vs30) + a_3.precipitation + a_4.distance\ to\ wate + a_5\ .water\ table\ depth \quad (2)$$

Where the coefficients are listed in Table 1.

Table 1. Variables' coefficients used in the GGLM (Zhu et al., 2017)

Variable	Coefficient	unit
Ln(PGV)	0.334	cm/ s
Ln(Vs_{30})	-1.918	m/s
Precipitation	5.408^{-4}	mm
Distance to Water	-0.2054	km
Water table Depth	-0.0333	m

The liquefaction probability (P) is then converted to liquefaction spatial extent (LSE) using equation 3 as introduced by Zhu et al.(2017):

$$\text{LSE(P)} = \frac{49.15}{\left(1+42.4e^{-9.165(P)}\right)^2} \quad (3)$$

Where P is the probability of liquefaction calculated by equation 1. This equation was derived by comparing probability values with observed liquefaction spatial extent from earthquakes with spatially complete maps (as discussed in Zhu et al., 2017). Liquefaction spatial extent (LSE) after an earthquake is the spatial area covered by surface manifestations of liquefaction reported as a percentage. In this study, the GGLM has been evaluated on 53 earthquakes around the globe and 6 different regions as described in Table 1.

Table 1. Summary of the earthquake events used in this study

Region	Date (dd/mm/year)	Magnitude (Mw)	Earthquake Name	Coastal / Non-coastal	Liquefaction occurrence	Spatial Completeness	Reference
North America	4/29/1965	6.7	Puget Sound	Coastal	Yes	Incomplete	Chleborad and Schuster (1990)
	10/17/1989	6.9	Loma Prieta	Coastal	Yes	Incomplete	Holzer (1998)
	1/17/1994	6.7	Northridge	Non Coastal	Yes	Incomplete	Stewart et al. (1994)
	10/16/1999	7.1	Hector Mine	Non Coastal	No	Complete	------
	3/9/2000	5	Yountville	Coastal	No	Complete	------
	2/28/2001	6.8	Nisqually	Coastal	Yes	Incomplete	Bray et al. (2001)
	11/3/2002	7.9	Denali	Non Coastal	Yes	Incomplete	Kayen et al. (2004)
	1/22/2003	7.5	Tecoman	Non Coastal	Yes	Incomplete	Wartman et al. (2005)
	12/22/2003	6.5	San Simeon	Coastal	Yes	Complete	Holzer et al. (2005)
	7/29/2008	5.4	Chino Hills	Coastal	No	Complete	------
	4/4/2010	7.2	Baja California	Non Coastal	Yes	Incomplete	Stewart and Brandenberg (2010)
	8/23/2011	5.8	Virginia	Non Coastal	Yes	Complete	Carter and Maurer
	8/24/2014	6	Napa	Coastal	Yes	Complete	Bray et al. (2014)
	8/17/2015	4	Piedmont	Coastal	No	Complete	------
	9/3/2016	5.8	Oklahoma	Non Coastal	Yes	Complete	Clayton et al. (2016)
South America	6/23/2001	8.4	Arequipa	Coastal	Yes	Complete	Gomez et al. (2005)
	8/15/2007	7.9	Pisco	Coastal	Yes	Complete	Taucer et al. (2009)
	2/27/2010	8.8	Maule	Coastal	Yes	Incomplete	Verdugo (2011)
	4/1/2011	8.2	Iquique	Coastal	Yes	Complete	Rollins et al. (2014)
	9/16/2015	8.3	Illapel	Coastal	Yes	Complete	Candia et al. (2015)
	4/16/2016	7.8	Muisne	Coastal	Yes	Incomplete	Nikolau et al. (2016)
Central America	4/22/1991	7.6	Telire Limon	Non Coastal	Yes	Incomplete	Yasuda et al. (1993)
	5/28/2009	7.3	Honduras	Coastal	Yes	Incomplete	Luna (2010)
	1/12/2010	7	Haiti	Coastal	Yes	Incomplete	Olsen et al. (2011)
	9/5/2012	7.6	Samara	Coastal	Yes	Incomplete	Rollins et al. (2013)

Table 1 (continued)

Region	Date (dd/mm/year)	Magnitude (Mw)	Earthquake Name	Coastal / Non-coastal	Liquefaction occurrence	Spatial Completeness	Reference
Europe	8/17/1999	7.6	Kocaeli	Coastal	Yes	Incomplete	Rathji et al. (2004)
	11/12/1999	7.2	Duzce	Non Coastal	Yes	Incomplete	Sucuoğlu (2000)
	6/8/2008	6.5	Achia	Coastal	Yes	Complete	Pavlides (2013)
	4/6/2009	6.3	Aquila	Non Coastal	Yes	Complete	Monaco (2011)
	10/23/2011	7.1	VanTab	Non Coastal	Yes	Complete	Erdik (2012)
	5/20/2012	6	Emilia	Non Coastal	Yes	Incomplete	Papathanassiou (2012)
	1/26/2014	6.1	Cephonia	Coastal	Yes	Complete	Papathanassiou (2016)
	8/24/2016	6.2	Central Italy	Non Coastal	No	Complete	Zimmaro and Stewart (2016)
Asia & Oceania	9/21/1999	6.3	Chi-Chi	Non Coastal	Yes	Incomplete	Yuan et al. (2004)
	1/26/2001	7	Bhju	Non Coastal	Yes	Incomplete	Bardet et al. (2001)
	5/12/2008	6.3	Wenchuan	Non Coastal	Yes	Incomplete	Huang and Jiang (2010)
	9/4/2010	7	Darfield	Coastal	Yes	Complete	Cubrinovski et al. (2010)
	2/22/2011	6.1	Christchurch	Coastal	Yes	Complete	Cubrinovski et al. (2011)
	4/25/2015	7.8	Kathmandu	Non Coastal	Yes	Incomplete	Hashash (2015)
	2/6/2016	6.3	Meinong	Coastal	Yes	Incomplete	Sun et al. (2016)
Japan	6/16/1964	7.6	Nigata	Coastal	Yes	Incomplete	Ishihara and Koga (1981)
	6/12/1978	7.7	Miyagi ken	Coastal	Yes	Incomplete	Tohno and Yasuda (1981)
	5/26/1983	7.7	Nihonkai	Coastal	Yes	Incomplete	Tohno and Shmoto (1985)
	7/12/1993	7.7	Hokkaido	Coastal	Yes	Incomplete	Miura et al. (1995)
	1/17/1995	6.9	Hyogoken Nambu	Coastal	Yes	Complete	Hamada et al. (1996)
	10/6/2000	6.7	Tottori	Coastal	Yes	Incomplete	Kiyono et al. (2007)
	9/26/2003	8.3	Tokaichi	Coastal	Yes	Incomplete	Wakamatsu (2011)
	10/23/2004	6.6	Nigata	Coastal	Yes	Incomplete	Rathji et al. (2006)
	7/16/2007	6.6	Nigata	Coastal	Yes	Incomplete	Kayen et al. (2009)
	6/14/2008	6.9	Iwate	Non Coastal	No	Incomplete	Kayen et al. (2008)
	3/11/2011	9.1	Tohoku	Coastal	Yes	Incomplete	Bhattacharya et al. (2011); Goto et al. (2012)
	4/14/2016	6.2	Kumamanto	Coastal	Yes	Incomplete	Mukunoki et al. (2016)

This dataset includes the 26 original events that were used for developing the model (Zhu et al. 2017) as well as 27 additional events that were chosen both to expand coverage globally and to include recent events. The GGLM was developed using 26 events from Japan, New Zealand, the United States, China and Taiwan (Zhu et al. 2017). This study expanded the validation of the GGLM to other global regions such as Italy, Turkey, Costa Rica, and Chile. These earthquakes were chosen to test the generality and regional efficacy of the model. While the majority of the new events are coastal as most of the tectonically active regions are near the coast, the model portability has also been tested on several non-coastal events. The majority of events were investigated by the Geotechnical Extreme Event Reconnaissance (GEER) efforts and therefore had information on field observations of liquefaction; however, the reports do not specifically talk about the spatial completeness of the reconnaissance efforts. Table 1 includes information about whether the field reconnaissance is known to be spatially complete. For the 27 new events, liquefaction occurrence is documented as discrete points with spatial reference derived from the reconnaissance reports; all the observed liquefaction points were either spatially mapped using their geographic coordinates or digitized through images and maps within the reports. Of the 27 new events, 25 events include liquefaction occurrence and 11 events are concluded to be spatially complete catalogs of liquefaction occurrence. Two events are included where no liquefaction was observed.

For each event, the extent of the GGLM prediction has been limited to the ShakeMap extent from USGS National Earthquake Information Center (downloaded from https://earthquake.usgs.gov/earthquakes). These maps provide estimates of ground shaking that integrate macroseismic data and available estimates of ground motion records measured with Ground Motion Prediction Equation (GMPE) (Worden et al., 2010). The ShakeMap provides PGA

and PGV estimates for the event. The global Vs_{30} layer has been estimated according to the method described in Wald and Allen (2007) which is based on elevation-derived slope. The Digital Elevation Model (DEM) for the globe has been accessed through Global Multi-resolution Terrain Elevation Data (2010). The distance to river (and lake) layer has been computed globally by using the Hydrological data from SHuttle Elevation Derivatives at multiple Scale (Hydro-SHEDS) which is based on topography. The distance to coast layer has been computed from a global dataset by National Aeronautics and Space Administration (NASA)'s Ocean Color Group. The distance to the nearest water body layer is defined as the minimum of distance to coast and distance to river and lake layers. The global precipitation layer has been created by bilinearly interpolating more than 40000 stations across the world averaging over 1959-2000 from WorldClim database (Zhu et al, 2017). Finally, the global ground water depth layer has been extracted from Fan et al. (2013) who modeled groundwater flow by using climate, terrain and see level data. Figure 1 shows each of the geospatial explanatory variables (event-independent) as well as shaking variables (PGA and PGV) for the 2011 Mineral, Virginia earthquake. As can be seen, the extent of USGS ShakeMap for the 2011 Mineral earthquake is large (roughly 400 km by 400 km).

Each of the model variables are stored as global layers in the World Geographic Coordinate System 1984 (WGS1984) and have a resolution of 30 arc-sec (~900 meters on Equator). For this work, each layer has been resampled to 3 arc-sec (~100 meters on Equator) using bilinear interpolation. Using lower resolution (30 arc-sec) works at the loss estimation scale but is insufficient for validation against liquefaction occurrence especially in coastal areas where higher resolution is needed. Bilinear resampling is appropriate to increase the resolution for continuous variables. Once the model variables are resampled to 3 arc-sec, they are projected through Albers equal-area conic to minimize the distortion of pixel area and create pixels equal

with a dimension of 100 meters. After resampling the explanatory variables within each event-specific extent, the liquefaction spatial extent is estimated using equations 1 through 3.

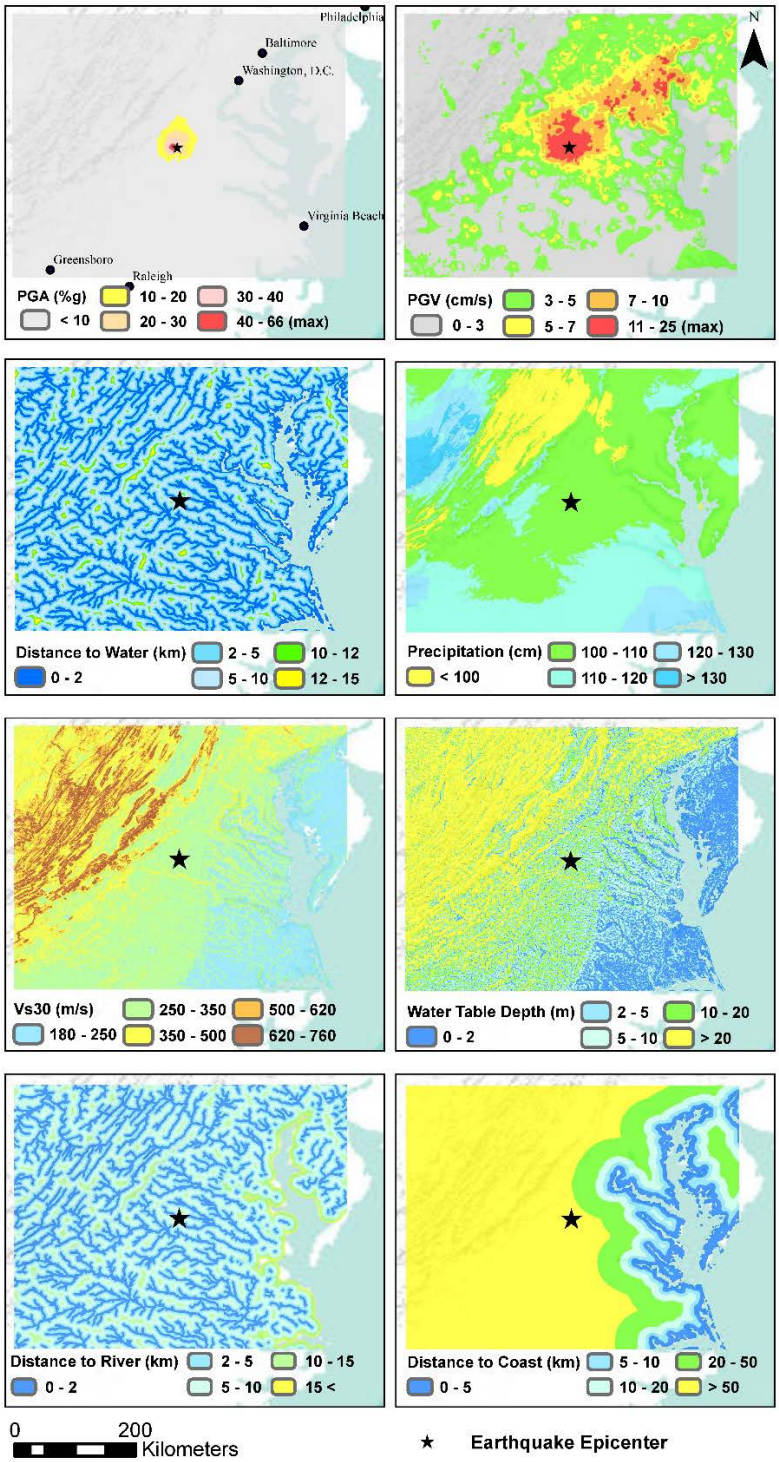

Figure 1. Explanatory variables used in the GGLM for the 2011 Mineral, Virginia earthquake.

As equation 3 estimates the spatial extent of liquefaction occurrence as a percent, the total expected liquefaction spatial extent (LSE) in the region can be estimated by summing the total area within individual pixels. When the spatial extent of liquefaction estimated from equation 3 is less than 0.5% of the pixel size, it is assigned a zero value; this ensures that the total summed LSE over a region does not get large by summing the pixels with liquefaction probability close to zero. Figure 2 shows the probability of liquefaction as well as the liquefaction spatial extent for 2011 Mineral, Virginia earthquake estimated by the GGLM.

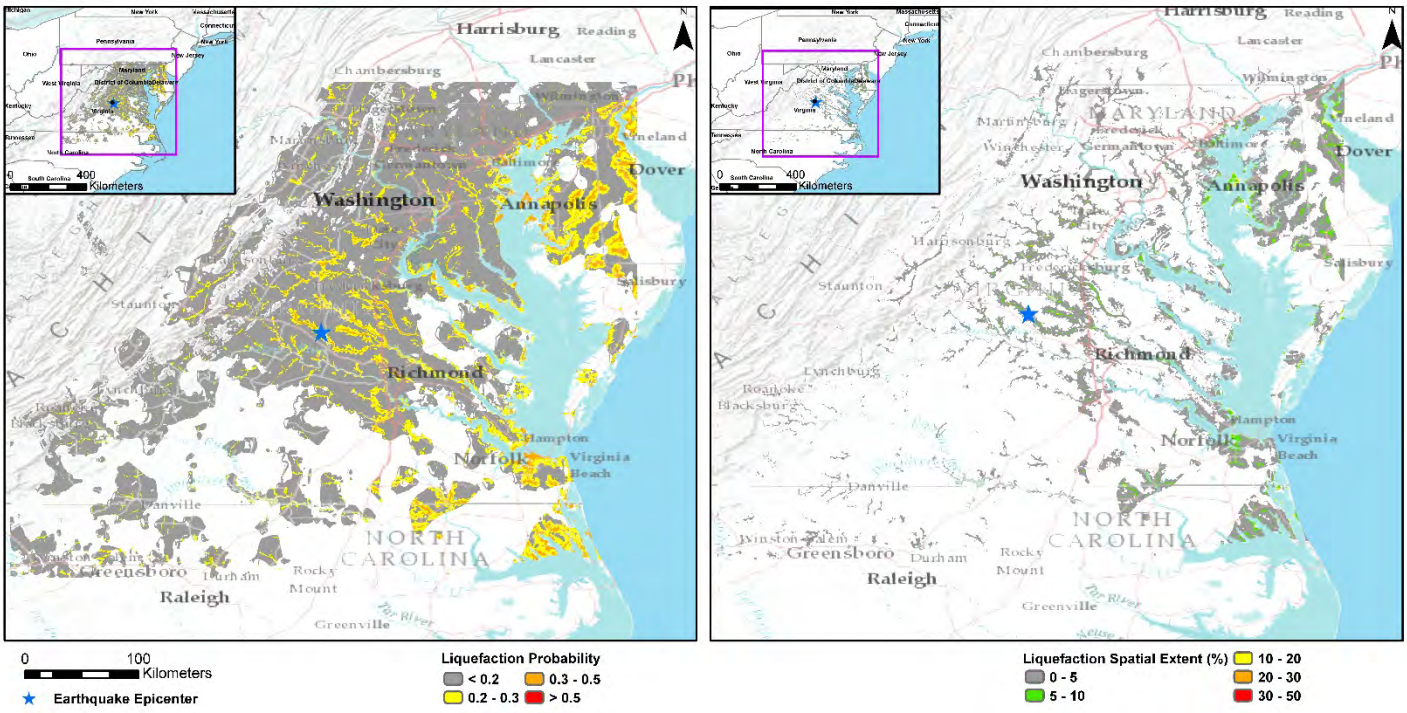

Figure 2. Liquefaction probability and liquefaction spatial extent after 2010 Mineral, Virginia earthquake estimated by the GGLM.

3.1. Model Modifications

During the validation of the GGLM, we realized that the liquefaction probability and spatial extent of liquefaction were over-predicted at large epicentral distances as exemplified in Figure 2 for the 2011 Mineral Earthquake and in Figure 3 for the 1989 Loma Prieta, 2007 Pisco and 2001 Nisqually earthquake. For each of these events, the reconnaissance efforts (roughly equals small box within the maps) did not identify liquefaction at these distances. For example, during the 2011 Mineral, Virginia earthquake, liquefaction occurrence was only observed close to the epicenter and was not observed in Washington D.C., Baltimore or along the coast of Delaware. To address the model over-prediction we examined the shaking variables PGA and PGV as shown in Figure 4. Zhu et al. (2017) demonstrated that observed liquefaction occurrences were consistent with a PGA and PGV value greater than 0.1g and 7 cm/s, respectively; however, the original GGLM does not capture the sharp step-functions observed in the plots for PGA and PGV. Because the PGV threshold was defined as part of the GGLM development, we have added a second threshold using PGA of 0.1g to better define the step-function behavior. Therefore, the GGLM was altered as follows:

$$P(x) = \begin{cases} \dfrac{1}{1+e^{-X}} & \text{If PGV > 3 cm/s AND PGA > 0.1g AND Vs30 < 620 m/s} \\ 0 & \text{Otherwise} \end{cases} \quad (4)$$

Where X is still calculated according to equation 2. Figure 5 presents the same four earthquakes shown in Figure 3 with the new PGA threshold as described in equation 4. In Figures 3 and 5, the black dots show the observed liquefaction points by reconnaissance team.

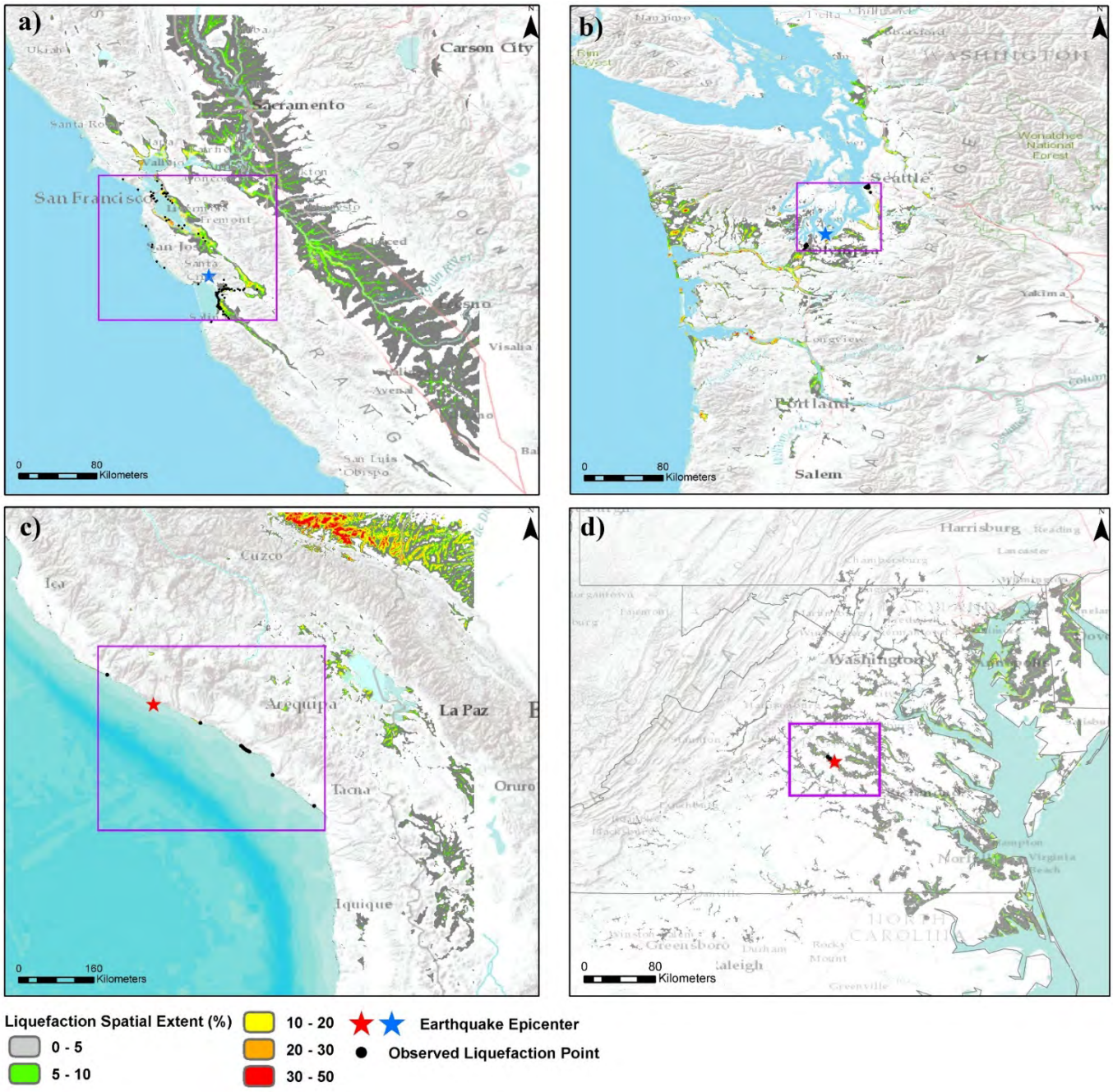

Figure 3. Liquefaction spatial extent for a) 1989 Loma Prieta, CA b) 2001 Nisqually, WA c) 2001 Pisco, Peru d) 2011 Mineral, VA earthquakes estimated by the GGLM enforcing PGV = 3 cm/s threshold.

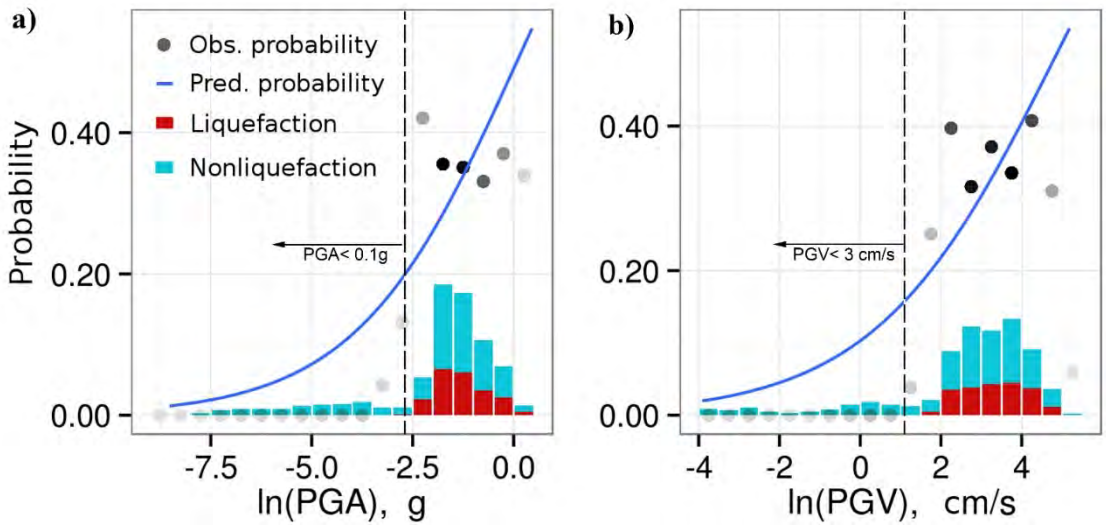

Figure 4. Histograms of liquefaction and non-liquefaction and the probability of liquefaction observed from the data (gray circles) at intervals of a variable's value and the probability predicted from a univariate model. The darkness of the gray dot increases with the number of data points within the bin (modified after Zhu et. al, 2017).

As observed from Figures 3 and 5, the PGA threshold of 0.1g results in LSE that is more consistent with the extent of observed by the reconnaissance team s. For example, for the Loma Prieta earthquake, all the observed liquefaction points are spatially predicted by the GGLM using PGA threshold of 0.1g. For the 2001 Pisco earthquake in Peru, the GGLM with the original PGV and Vs30 thresholds predicts liquefaction far from the coast while liquefaction was only reported near the coast.

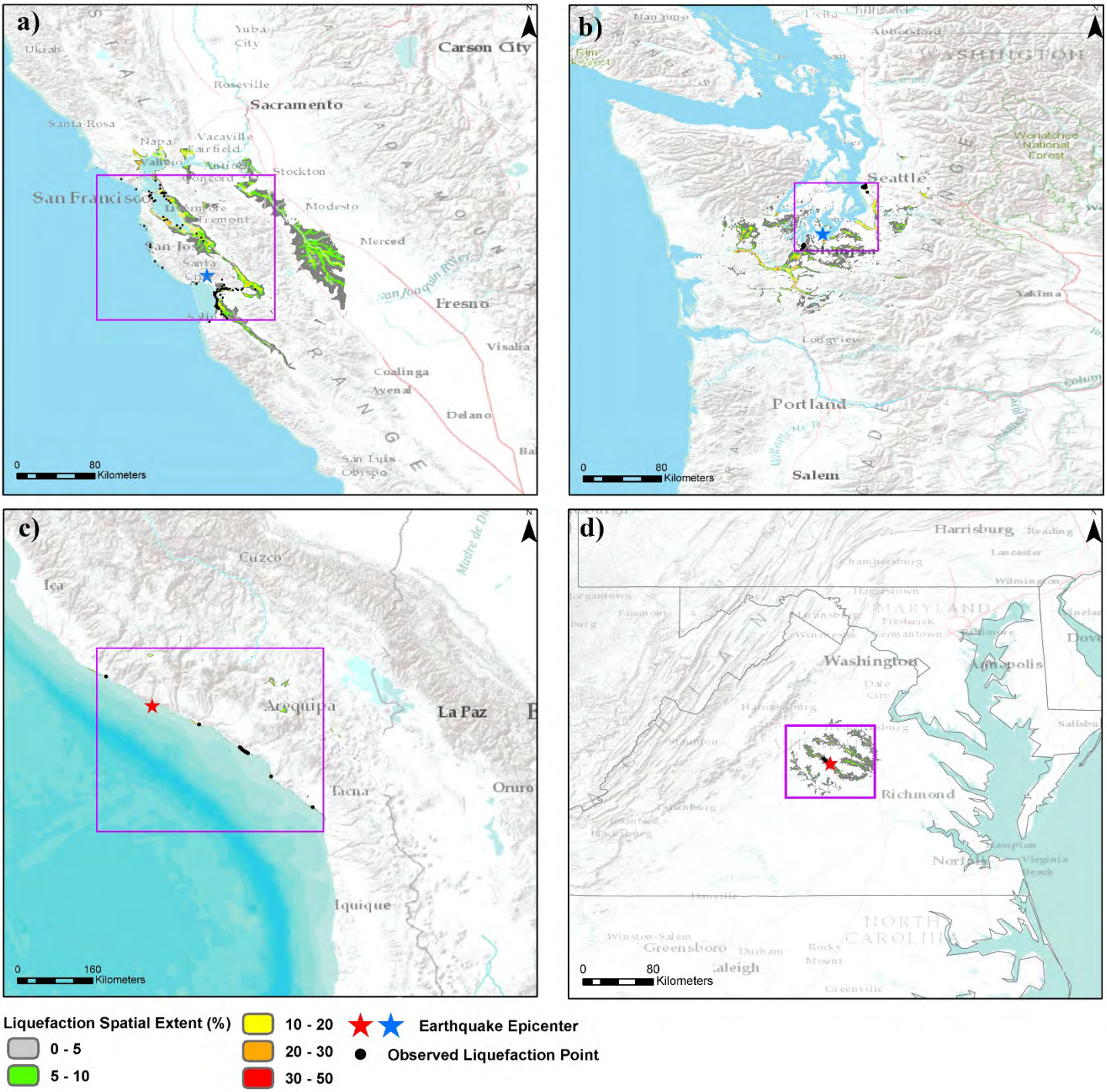

Figure 5. Liquefaction spatial extent for a) 1989 Loma Prieta, CA b) 2001 Nisqually, WA c) 2001 Pisco, Peru d) Mineral, VA earthquakes estimated by the GGLM enforcing PGV = 3 cm/s AND PGA = 0.1g thresholds.

After modifying the GGLM to include the new PGA threshold, all 53 earthquakes have been evaluated using the modified GGLM and liquefaction spatial extent (LSE) has been calculated according to equation 3. The results of the analyses are discussed in the following section.

4. Results and discussion

Model performance is evaluated by comparing predicted LSE with field observations of liquefaction. Because liquefaction observations are generally not complete for the earthquakes in the database, each earthquake is given a qualitative rating on observed liquefaction intensity based on the field observation report as shown in Table 2. LSE is calculated with the modified GGLM and summed for each earthquake. Table 3 presents the LSE score and liquefaction intensity for each earthquake.

Table 2. Description of the liquefaction occurrence based on field observation

Liquefaction intensity	Description
1-No to minor	No liquefaction or few to several points of sand boils are observed close to coast or water streams; structural damage is rare.
2-Minor to moderate	Different types of liquefaction and lateral spread are observed; mostly close to coastal zones and water streams; structural damage expected;
3-Moderate to severe	Different types of liquefaction and lateral spread are observed; liquefied ejecta are frequent on the ground. Structural damage and failure occur. Liquefaction observations are usually localized and not reported far distance from each other.
4-Severe to extensive	Different types of liquefaction and lateral spread are observed; liquefaction is frequent in large extent and can be observed from aerial flight. Damaged and failed structures are easy to find; Liquefaction is reported in multiple cities and far distance from each other and epicenter.

Table 3. Summary of the model prediction and liquefaction observation of the earthquakes used in the study.

Region	Date (dd/mm/year)	Magnitude (Mw)	Earthquake Name	Coastal / Non-coastal	Liquefaction occurrence	LSE Score (km^2)	Liquefaction Intensity Class
North America	4/29/1965	6.7	Puget Sound	Coastal	Yes	319	3
	10/17/1989	6.9	Loma Prieta	Coastal	Yes	277	3
	1/17/1994	6.7	Northridge	Non Coastal	Yes	48	1
	10/16/1999	7.1	Hector Mine	Non Coastal	No	52	1
	3/9/2000	5	Yountville	Coastal	No	2	1
	2/28/2001	6.8	Nisqually	Coastal	Yes	111	2
	11/3/2002	7.9	Denali	Non Coastal	Yes	88	3
	1/22/2003	7.5	Tecoman	Non Coastal	Yes	87	2
	12/22/2003	6.5	San Simeon	Coastal	Yes	4	1
	7/29/2008	5.4	Chino Hills	Coastal	No	2	1
	4/4/2010	7.2	Baja California	Non Coastal	Yes	434	4
	8/23/2011	5.8	Virginia	Non Coastal	Yes	28	1
	8/24/2014	6	Napa	Coastal	Yes	27	1
	8/17/2015	4	Piedmont	Coastal	No	0	1
	9/3/2016	5.8	Oklahoma	Non Coastal	Yes	22	1
South America	6/23/2001	8.3	Arequipa	Coastal	Yes	47	1
	8/15/2007	8	Pisco	Coastal	Yes	13	1
	2/27/2010	8.8	Maule	Coastal	Yes	1510	4
	4/1/2011	8.2	Iquique	Coastal	Yes	41	1
	9/16/2015	8.3	Illapel	Coastal	Yes	42	1
	4/16/2016	7.8	Ecuador	Coastal	Yes	2391	4
Central America	4/22/1991	7.6	Telire Limon	Non Coastal	Yes	1856	4
	5/28/2009	7.3	Honduras	Coastal	Yes	992	4
	1/12/2010	7	Haiti	Coastal	Yes	332	3
	9/5/2012	7.6	Samara	Coastal	Yes	1397	4

Table 3 (continued)

Region	Date (dd/mm/year)	Magnitude (Mw)	Earthquake Name	Coastal / Non-coastal	Liquefaction occurrence	LSE Score (km^2)	Liquefaction Intensity Class
Europe	8/17/1999	7.6	Kocaeli	Coastal	Yes	231	3
	11/12/1999	7.2	Duzce	Non Coastal	Yes	39	2
	6/8/2008	6.5	Achia	Coastal	Yes	68	2
	4/6/2009	6.3	Aquila	Non Coastal	Yes	16	1
	10/23/2011	7.1	VanTab	Non Coastal	Yes	51	2
	5/20/2012	6	Emilia	Non Coastal	Yes	28	2
	1/26/2014	6.1	Cephonia	Coastal	Yes	2	1
	8/24/2016	6.2	Central Italy	Non Coastal	No	0	1
Asia & Oceania	9/21/1999	6.3	Chi-Chi	Non Coastal	Yes	701	4
	1/26/2001	7	Bhju	Non Coastal	Yes	8834	4
	5/12/2008	6.3	Wenchuan	Non Coastal	Yes	448	4
	9/4/2010	7	Darfield	Coastal	Yes	208	3
	2/22/2011	6.1	Christchurch	Coastal	Yes	64	3
	4/25/2015	7.8	Kathmandu	Non Coastal	Yes	1853	3
	2/6/2016	6.3	Meinong	Coastal	Yes	437	4
Japan	6/16/1964	7.6	Nigata	Coastal	Yes	487	4
	6/12/1978	7.7	Miyagi ken	Coastal	Yes	770	3
	5/26/1983	7.7	Nihonkai	Coastal	Yes	190	3
	7/12/1993	7.7	Hokkaido	Coastal	Yes	26	2
	1/17/1995	6.9	Hyogo Ken Na	Coastal	Yes	456	4
	10/6/2000	6.7	Tottori	Coastal	Yes	176	2
	9/26/2003	8.3	Tokaichi	Coastal	Yes	759	4
	10/23/2004	6.6	Nigata	Coastal	Yes	373	3
	7/16/2007	6.6	Nigata	Coastal	Yes	328	3
	6/14/2008	6.9	Iwate	Non Coastal	No	221	1
	3/11/2011	9.1	Tohoku	Coastal	Yes	2320	4
	4/14/2016	6.2	Kumamanto	Coastal	Yes	428	3

The range of predicted LSE in each liquefaction intensity class is shown in Figure 6. As can be seen, the median LSE increases as the liquefaction intensity increases. The median values for categories 1 to 4 are 25, 60, 320 and 900, respectively. Categories 1 to 3 have been enlarged and shown in the inner box of Figure 6. While categories 1 and 2 have overlap with each other, categories 2, 3 and 4 have mutually exclusive ranges if we use the whiskers to determine the range. LSE is a simple index that can be correlated with liquefaction intensity. For the purpose of classification, we decided to discriminate the LSE classes based on the value of 10^{th} percentile in each box and whicker plot; therefore, the liquefaction spatial extent value can be classified as presented in Table 4. According to this classification, 40 out of 53 earthquakes are classified correctly; all earthquakes in category 4 are classified correctly while 6 out of 13 mismatches belong to category 1; however, all these 6 earthquakes except 2008 Iwate event has LSE value between 40 to 50. Two out of 13 mismatches belong to category 2; one under classified and one over classified. The other 5 mismatches belong to category 3.

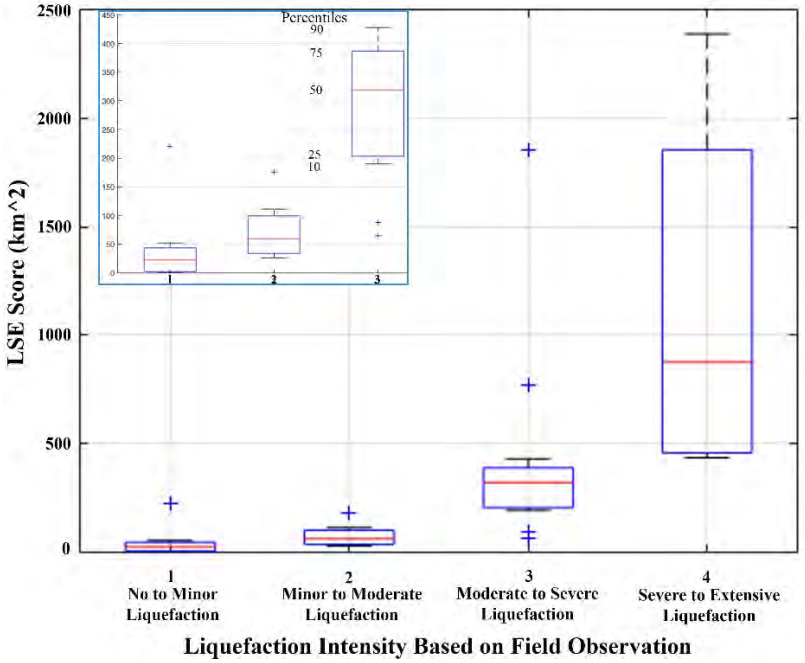

Figure 6. Box-and-Whisker plots for predicted LSE scores

Table 4. Classification of the LSE score into Liquefaction Intensity Classes

LSE Score (km^2)	Expected Liquefaction Intensity Class
< 30	1-No to minor
30-190	2-Minor to moderate
190-430	3-Moderate to severe
>430	4-Severe to extensive

4.1 Regional efficacy and performance of the model

As presented in Tables 1 and 3, the earthquake events have been categorized into 6 different regions in order to evaluate model performance regionally. For all 53 earthquakes, spatial performance of the model has been validated using observed liquefaction points recorded by the reconnaissance teams.

4.1.1 North America

Earthquakes in the North America region include events from Mexico to Alaska. While the majority of events in this region are coastal, there are a few earthquakes that occurred far from coast such as the 2002 Denali, Alaska event and the 2011 Mineral Virginia event. As presented in Table 2, for the earthquakes in which no or minor liquefaction was observed, the GGLM is predicting a LSE score close to zero. The spatial performance of the model for recent earthquakes in North America is shown in Figure 7 where the model performance for the majority of events is consistent with observations. For the Baja California earthquake in 2010 which has the highest predicted liquefaction spatial extent (in the north America region), the model has predicted liquefaction at all points that liquefaction was recorded by the reconnaissance team. The GGLM results for Oklahoma and Napa events where only limited liquefaction was observed are also

consistent; however, for the Hector mine earthquake although the model predicted 52 km of LSE, no liquefaction was observed.

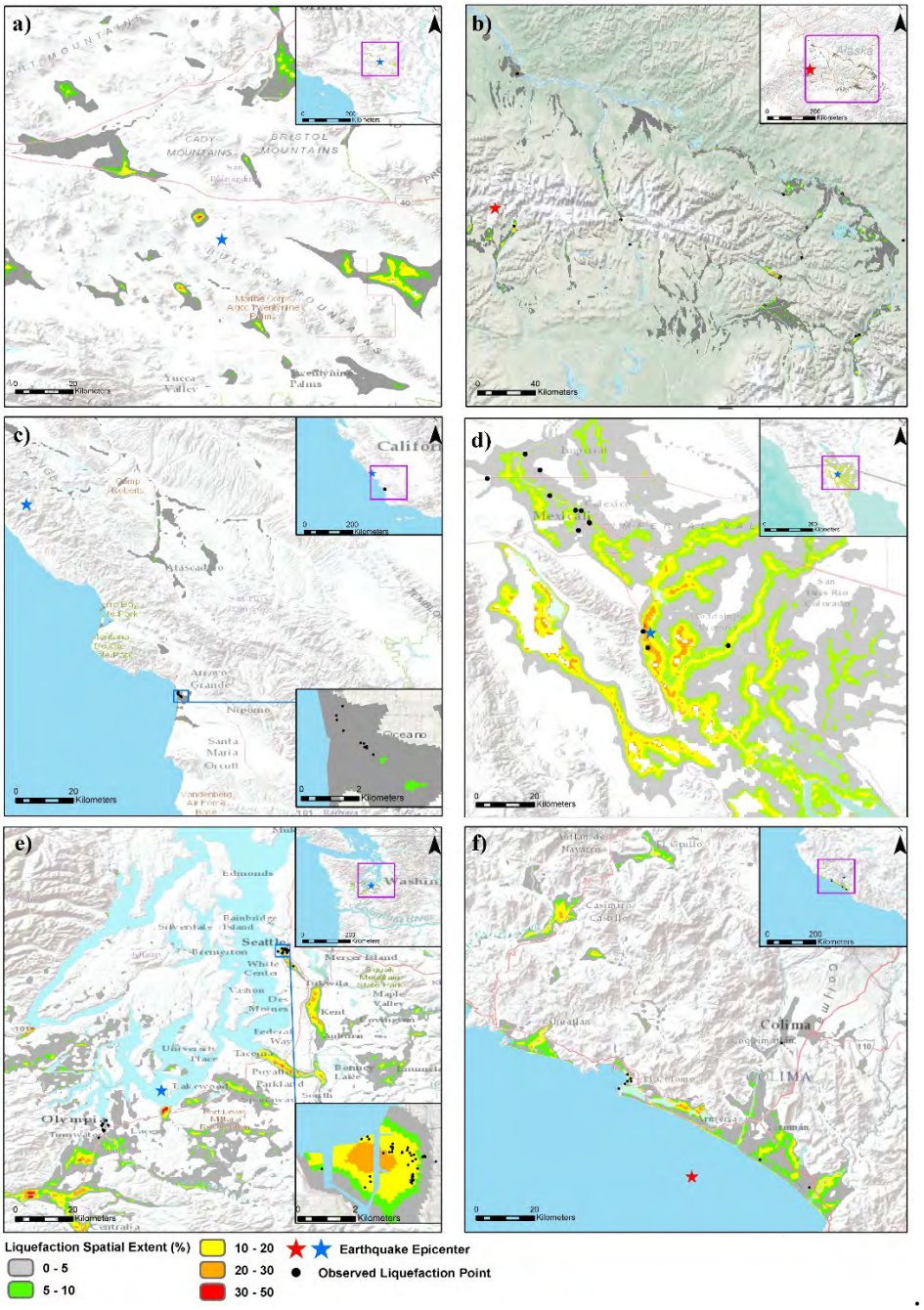

Figure 7. Spatial performance of the GGLM and LSE prediction for the recent earthquakes in North America: a) Hector Mine, 2001, b) Denali 2001, c) San Simeon 2003, d) Baja California 2010, e) Nisqually 2001, f) Tecoman 2003

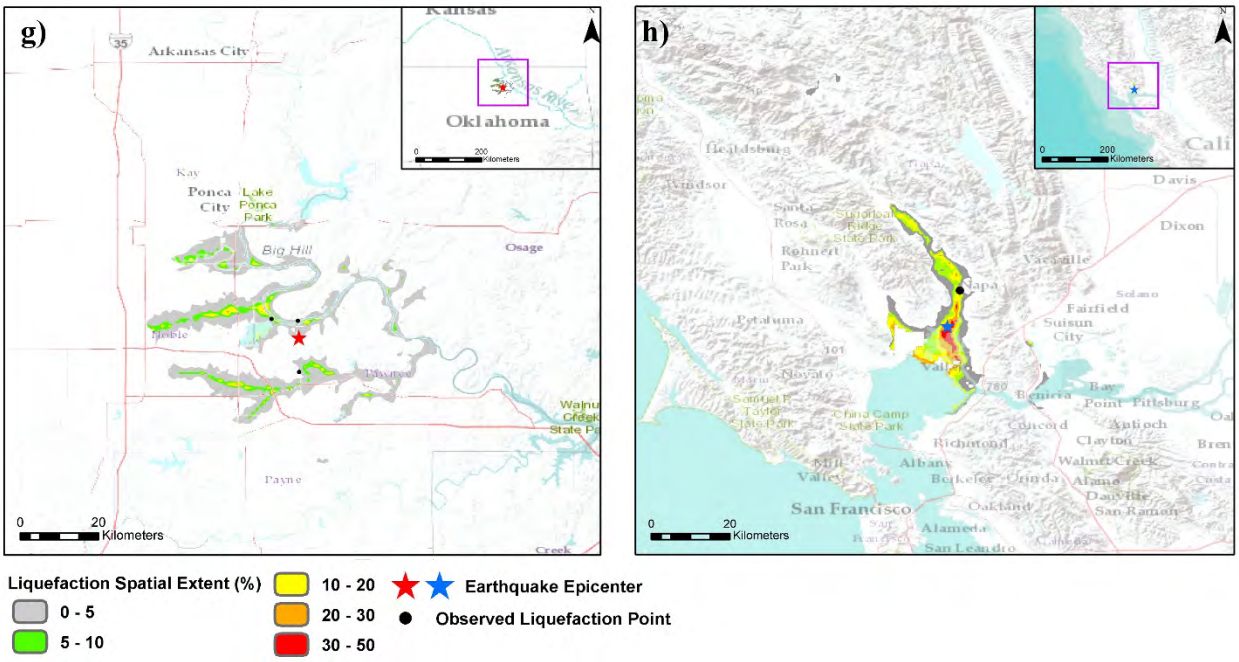

Figure 7 (continued). Spatial performance of the GGLM and LSE prediction for the recent earthquakes in North America: g) Oklahoma, 2016, h) Napa 2014

4.1.2 South America

There are six earthquakes in the database that have occurred in Chile, Peru and Ecuador. All earthquakes' epicenters are in Pacific Ocean and close to the coast of continent. For the earthquakes in Peru (Arequipa) and north of Chile (Illapel and Iquique), the model predicts low liquefaction relative to the area that holds PGA> 0.1g (as the rupture plane was huge, the area with PGA>0.1g was enormous); also the liquefaction extent predicted is mostly in the vicinity of coastal zone (which is in consistency with field observation reports). The main reason for low liquefaction prediction could be high value of Vs_{30} due to presence of Andes Mountains in this region close to the coast. As moving down toward south of Chile or up toward Ecuador, the Andes Mountains move inland and the flat foothills distance to the coast will increase; therefore, the value of Vs_{30} is low between the mountains and Pacific coast which increases the probability of liquefaction. In

Table 2 the Muisne and Maule Earthquakes in Ecuador and south of Chile have the highest predicted LSE in this region. As shown in Figure 8, the model is able to predict the spatial location of most of the liquefied points observed after the earthquakes but overpredicts away from the epicenter in the Muisne and Maule earthquakes (c and d).

4.1.3 Central America and Caribbean

There are four earthquakes in the database that have occurred in the Central America and Caribbean region. As presented in Table 2, the LSE score predicted by the model is high for all earthquakes in this region especially for the earthquakes in Costa Rica; this is consistent with the intensity of liquefaction reported by reconnaissance team where 3 out of 4 earthquakes have been classified as severe to extensive liquefaction. Figure 9 shows the spatial performance of the model for each earthquake as compared to the observed liquefaction points. Each of these earthquakes resulted in high predictions of LSE from the GGLM.

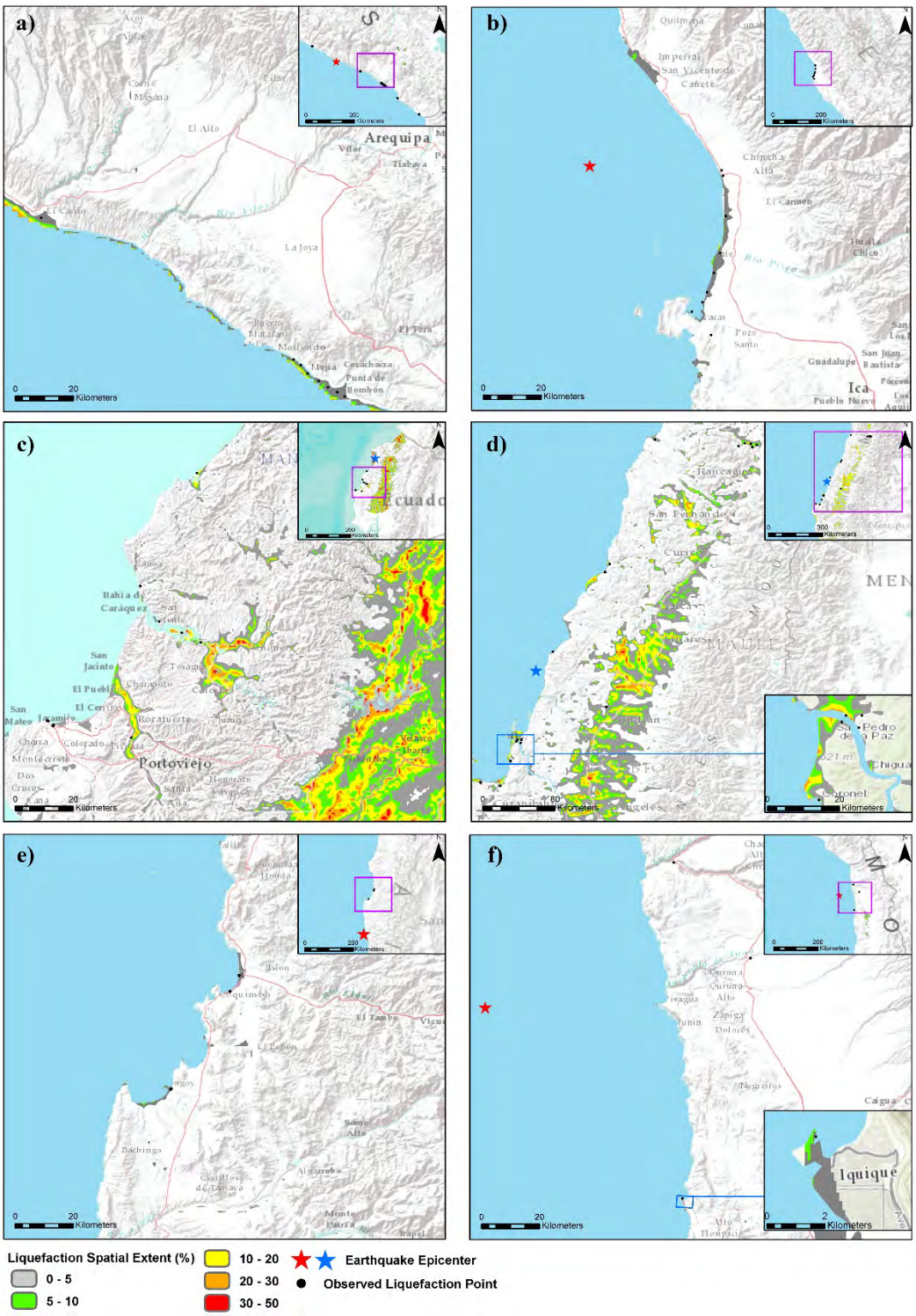

Figure 8. Spatial performance of the GGLM and LSE prediction for the recent earthquakes in South America: a) Arequipa, Peru 2001, b) Pisco, Peru 2007, c) Maule, Chile 2010, d) Muisne, Ecuador 2016, e) Illapel, Chile 2015, f) Iquique, Chile 2011

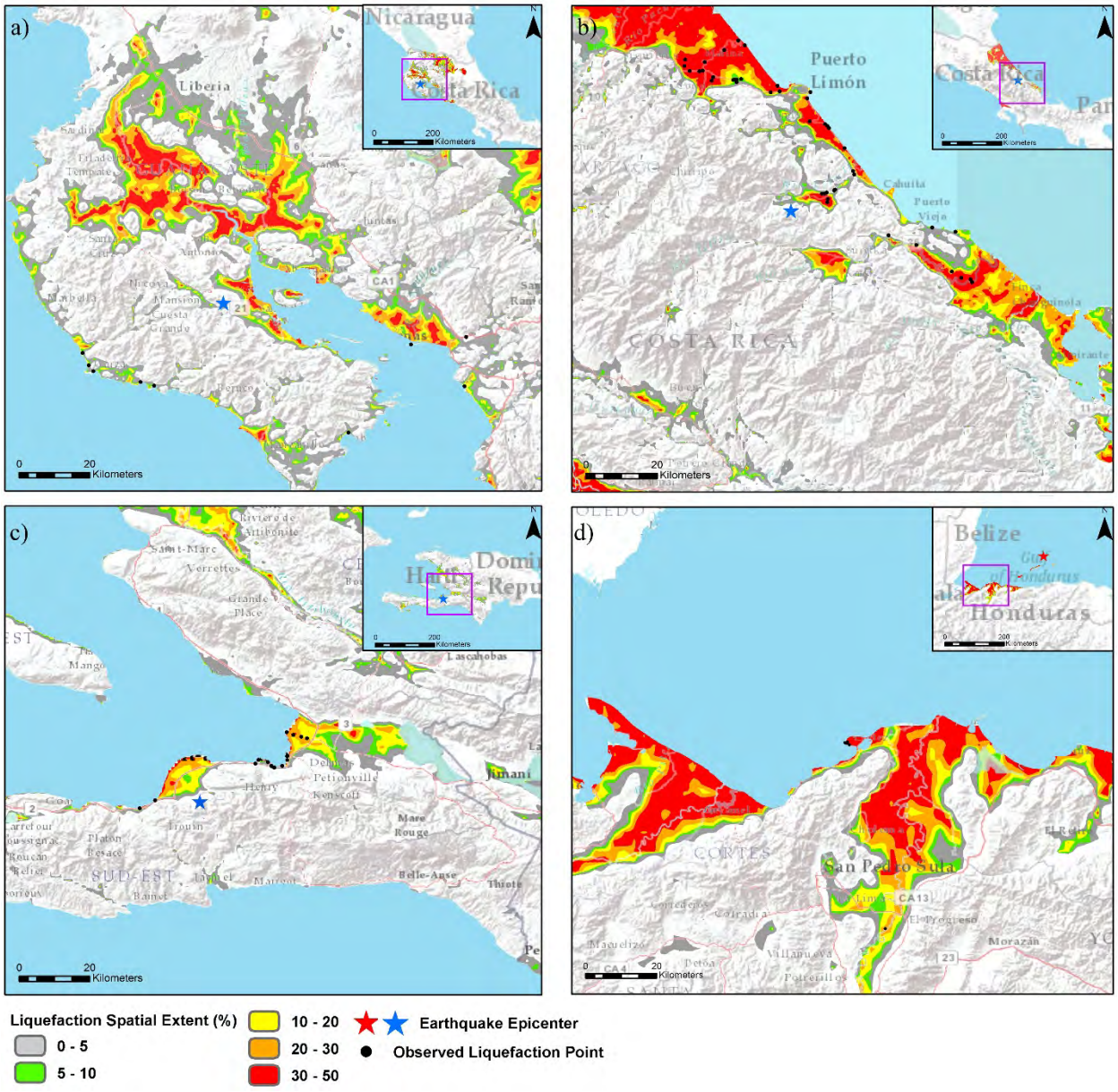

Figure 9. Spatial performance of the GGLM and LSE prediction for the recent earthquakes in Central America: a) Samara, Costa Rica 2012, b) Telire Limon, Costa Rica 1991, c) Haiti 2010, d) Honduras 2009

4.1.4 Europe

Italy, Greece and Turkey are countries in Europe that have experienced earthquakes recently. As presented in Table 2, while the majority of the events are non-coastal, liquefaction has been recorded in all events except the 2016 central Italy earthquake. For the earthquakes where

liquefaction was observed, the model has captured most of the observed liquefaction points (Figure 10). For the Kocaeli earthquake, the GGLM predicted the highest LSE score in the region which is consistent with the reconnaissance report which documented widespread liquefaction and ground failures. For the Cephonia earthquake in Greece, the area with PGA > 0.1g is small and therefore, the model prediction of LSE is low; however, even with this low liquefaction prediction, the model can capture most of the points in coastal zone that were marked by the reconnaissance team as liquefied. For the 2016 central Italy earthquake where no liquefaction was reported, the GGLM-based LSE is zero as presented in Table 2.

4.1.5 Asia and Oceania

Earthquakes in this region are in a wide geographic range from east of India to Taiwan and New Zealand. Earthquakes in India and Nepal have the highest predicted LSE scores in this region as presented in Table 2. As shown in Figure 11, the model predicts significant LSE after the Bhuj earthquake by capturing all alluvial channels in the mountainous region even far from epicenter. Although the reconnaissance did not cover this region, this is likely an overprediction of the GGLM. For the Taiwanese earthquakes, the model predicts a higher LSE score for the Chi-Chi 1999 event which is consistent with the field reports. For the New Zealand earthquakes, the model predicts higher LSE score for the 2010 Darfield event; however as shown in Figure 12 the model predicts higher spatial extent of liquefaction in the city of Christchurch and its vicinity after the Christchurch event in 2011 which is again consistent with the reconnaissance report of field observation after both events. The GGLM predictions in Kathmandu during the 2015 Nepal earthquake are spatially consistent with the reconnaissance reports. This is noteworthy that the reconnaissance team had anticipated more extensive liquefaction than observed.

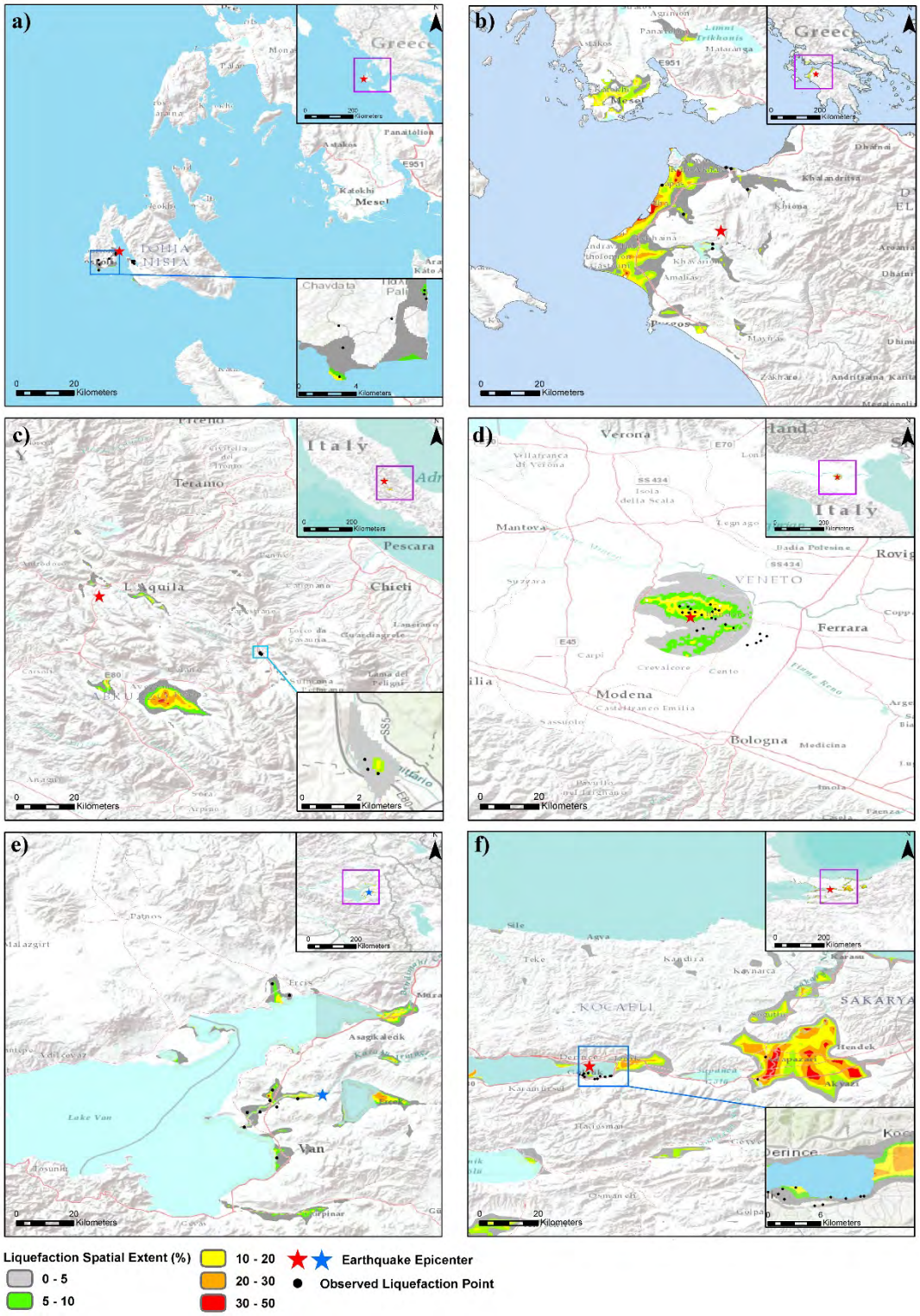

Figure 10. Spatial performance of the GGLM and LSE prediction for the recent earthquakes in Europe: a) Cephonia, Greece 2014, b) Achia, Greece 2008, c) Aquila, Italy 2009, d) Emilia, Italy 2012, e) VanTab, Turkey 2011, f) Kocaeli, Turkey 1999

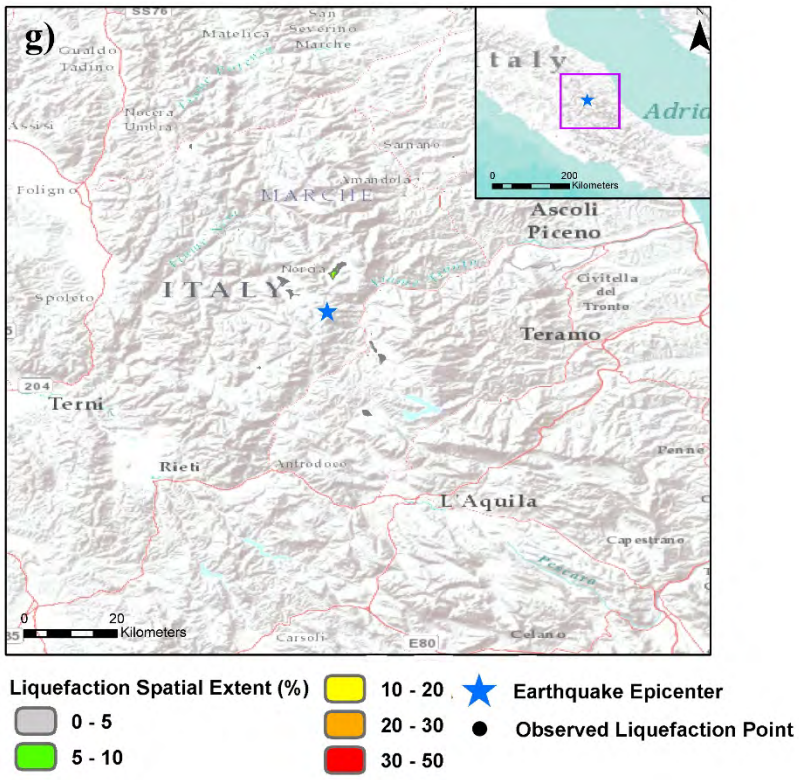

Figure 10 (continued). Spatial performance of the GGLM and LSE prediction for the recent earthquakes in Europe: g) Central Italy, 2016

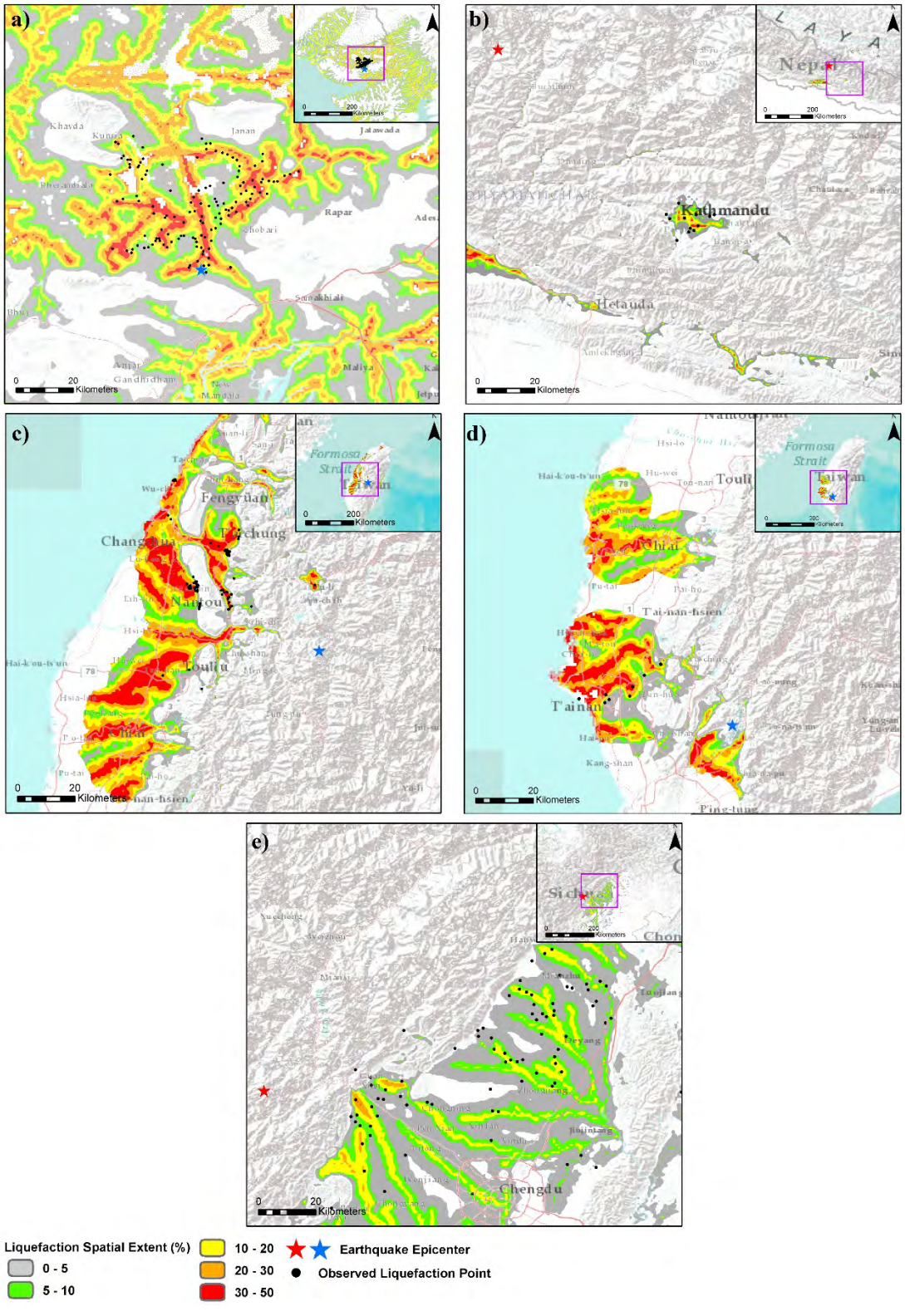

Figure 11. Spatial performance of the GGLM and LSE prediction for the recent earthquakes in Asia: a) Bhju, India 2001 b) Nepal 2015, c) ChiChi, Taiwan 1999, d) Meinong, Taiwan 2016, e) Wenchuan, China 2008

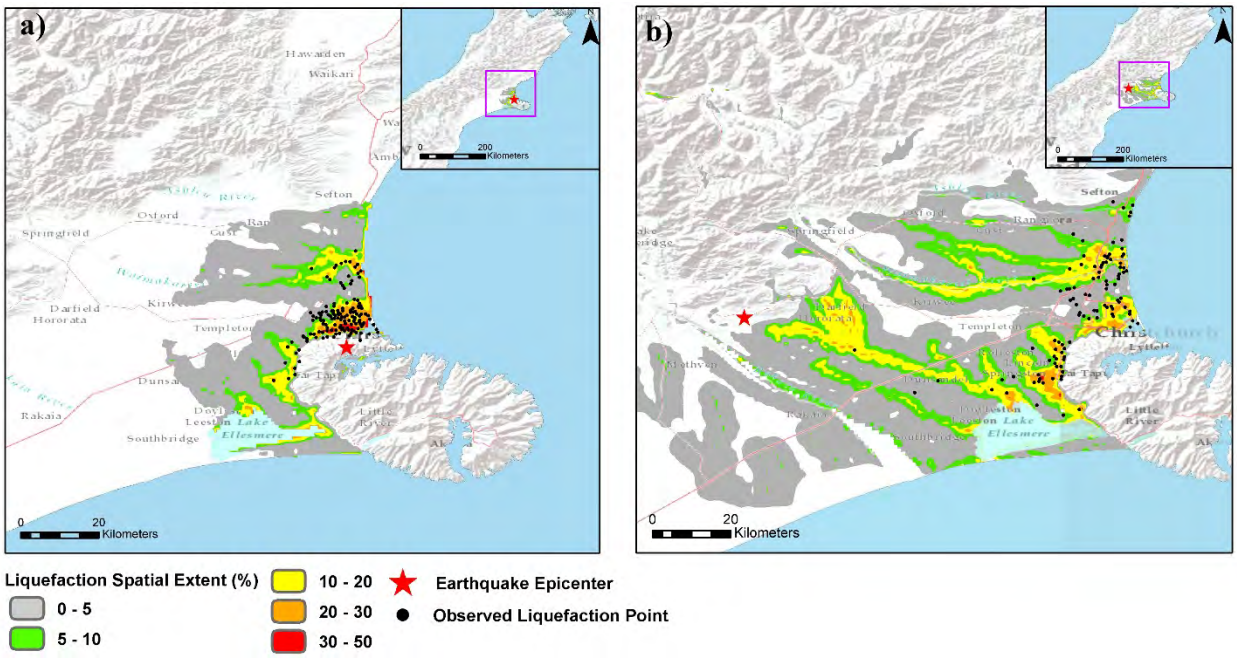

Figure 12. Spatial performance of the GGLM and LSE prediction for the recent earthquakes in New Zealand: a) Christchurch 2011 b) Darfield 2010

4.1.6 Japan

In the database, 11 out of 12 earthquakes in Japan region have experienced liquefaction. Only the 2008 Iwate earthquake, the only non-coastal event, did not include reports of liquefaction; however, there are cases of lateral spreads and pavement cracks in the reconnaissance report (one of them with geographical location has been mapped in Figure 13). The GGLM has predicted high LSE score for Iwate earthquake (Table 2). A majority of the area with PGA >0.1g is same as the area with PGA > 0.1g in the 1978 Miyagi Ken earthquake where many points of liquefaction were reported. The 2008 Iwate earthquake reconnaissance team reported that they were surprised to see no manifestation of liquefaction. For Japan, the GGLM has predicted the highest LSE for the Tohoku earthquake in 2010 which is in consistent with the reconnaissance reports of the events. As can be seen from Figure 13, the model has predicted liquefaction in large extent across the eastern coast of Japan after 2011 Tohoku earthquake.

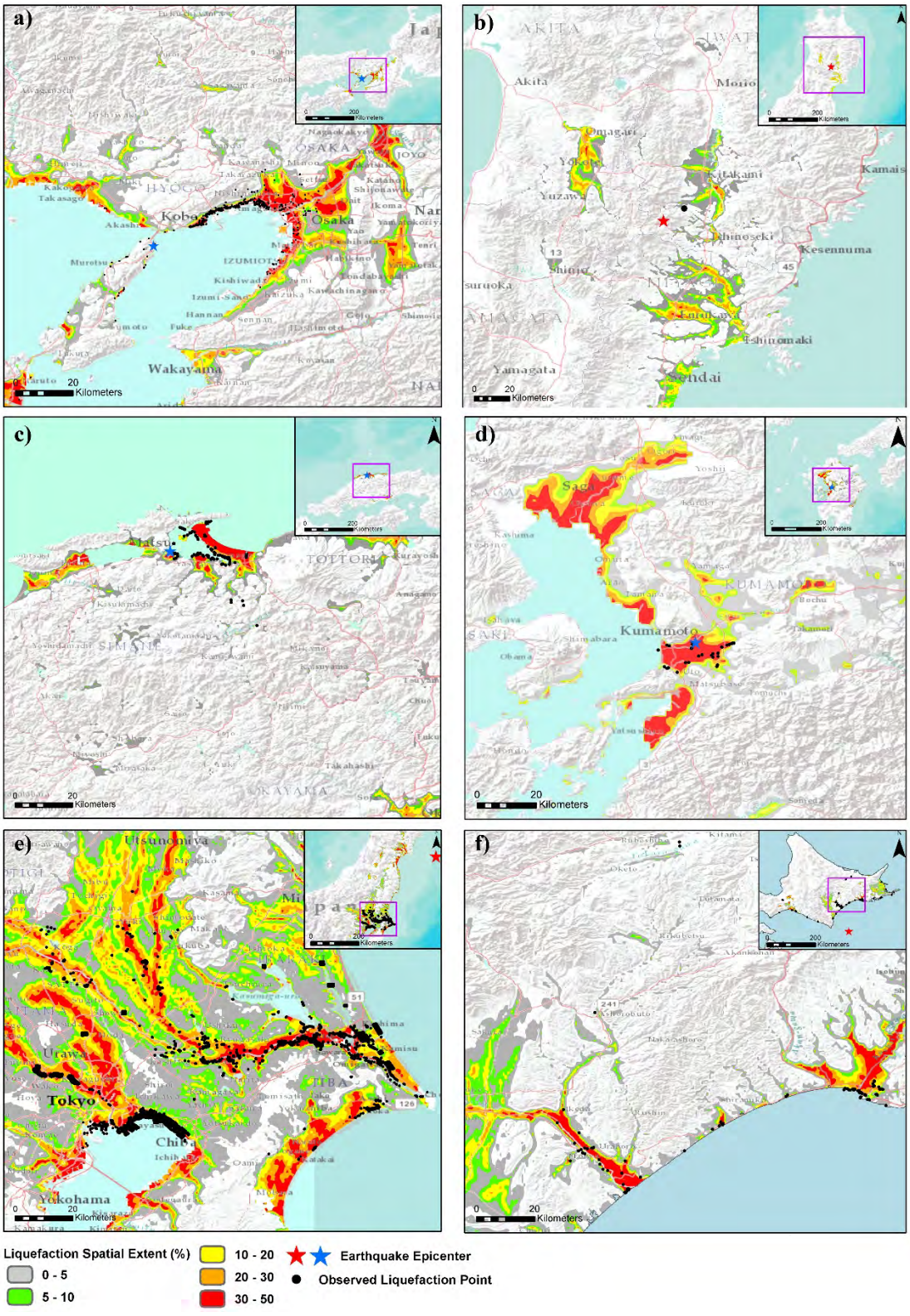

Figure 13. Spatial performance of the GGLM and LSE prediction for the recent earthquakes in Japan: a) Hyogoken Nambu 1995, b) Iwate 2008, c) Tottori 2000, d) Kumamoto 2016, e) Tohoku 2011, f) Tokaichi 2003

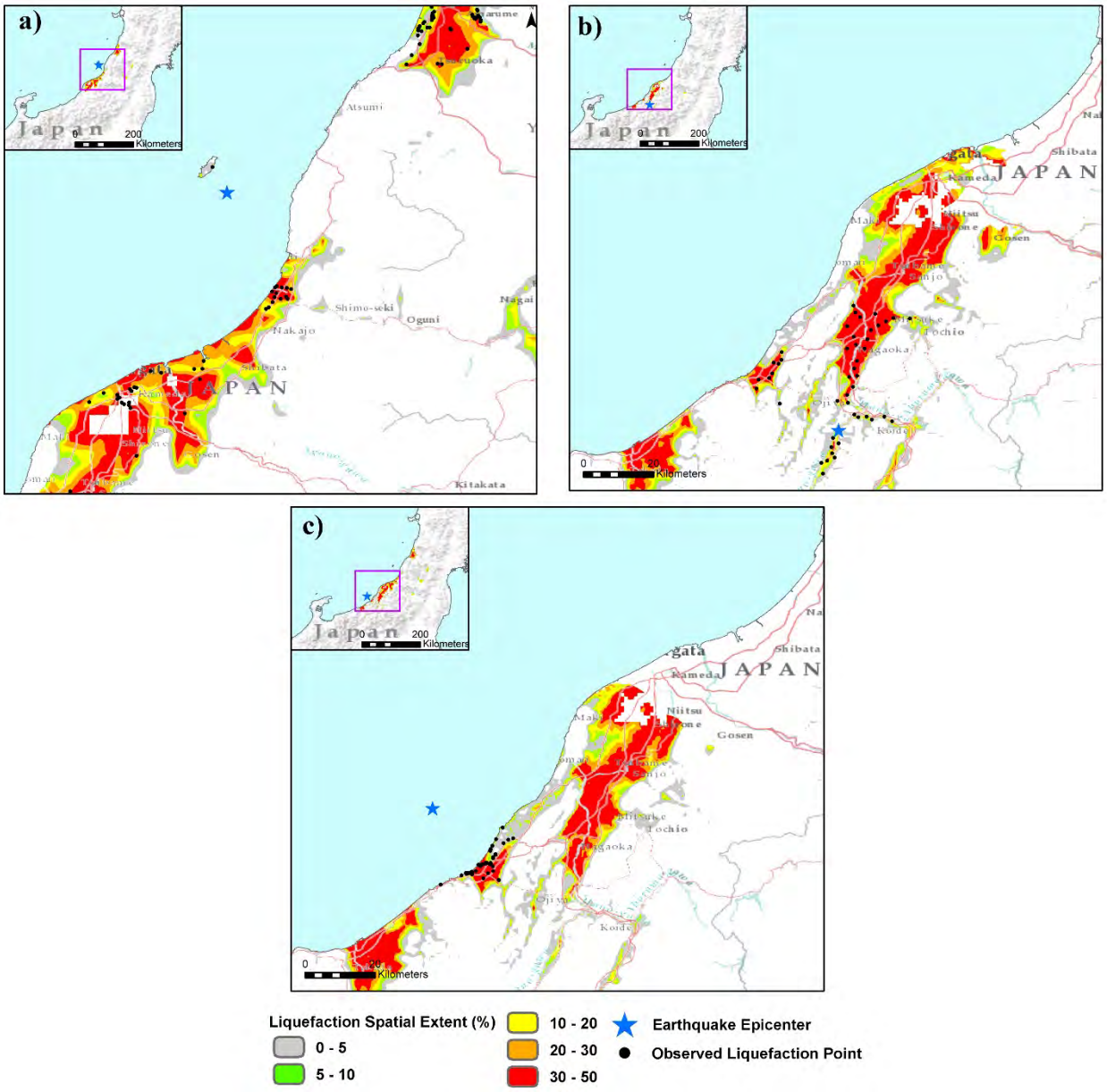

Figure 14. Spatial performance of the GGLM and LSE prediction for the earthquakes in Nigata, Japan: a) 1964, b) 2004, c) 2007

There are three earthquakes that have occurred in 1964, 2004, and 2007 in the Nigata area. Figure 14 shows the GGLM results and observed liquefaction for the three collocated earthquakes. The difference in LSE result from different patterns of the shaking parameters (PGA and PGV) as the other geospatial parameters are same for all three earthquakes. As presented in Table 2, the

1964 earthquake has the highest predicted LSE score which supports the reconnaissance reports of these three events.

4.2 Over saturation of the GGLM

As presented in Table 2, the value of LSE score for some earthquakes are higher than expected as a result of prediction of liquefaction by the GGLM at far epicentral distance. While the PGA threshold of 0.1g has been implemented in this study, it seems the model still overpredicts the occurrence of liquefaction in some regions, specifically Central America and India. While we do not have clear information on spatial completeness of the field observation of liquefaction, we expect that the GGLM may overpredict in some cases. We do not observe the same level of overprediction in North America and Europe. Figure 15 shows the extent of GGLM prediction of liquefaction for the four earthquakes with the highest LSE scores (except the 2011 Tohoku event) along with the observed liquefaction points and rough estimate of the areal extent examined by the reconnaissance team after each event (small blue boxes within the maps). The Tohoku earthquake in 2011 has a high LSE value but as liquefaction was extensive, the GGLM prediction is consistent with the observations. Part of the overprediction for these large Magnitude earthquakes may result from the significant area with PGA > 0.1g.

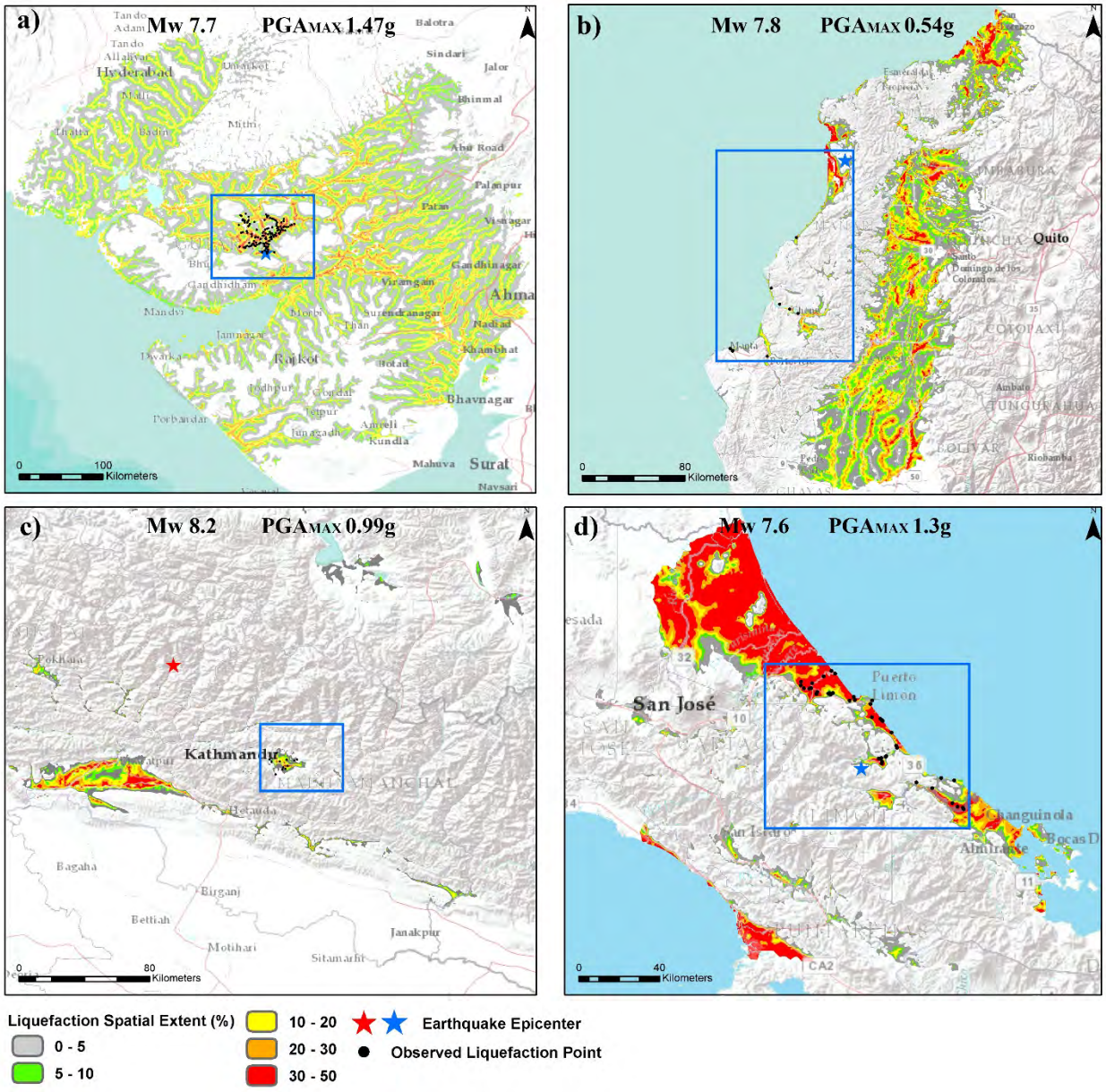

Figure 15. Spatial performance of the GGLM for the r earthquakes with highest LSE values: a) Bhuj, India 2001, b) Ecuador, 2016, c) Nepal, 2015, d) Telire Limon, 1991

4.3 Spatial performance of the model in urban scale

After the Christchurch earthquake in February 2011, widespread liquefaction was observed in the Christchurch City and its vicinity. Numerous types of geotechnical tests and data including hundreds of CPT have been conducted and collected (available at NZGD.org.nz). We have evaluated the spatial performance of the GGLM in the city of Christchurch and its vicinity where detailed field observation of liquefaction was conducted by comparing the predicted LSE with the Liquefaction Potential Index (LPI) and the property-by-property field observations of liquefaction. Iwasaki et al. (1978) defined the LPI according to Equation 4:

$$LPI = \int_0^{20m} F \cdot w(z) \cdot dz \tag{4}$$

Where F (defined in Equation 5) is a severity term equal to the amount by which the factor of safety (FS) against liquefaction triggering of a layer of soil is less than one, and $w(z)$ as shown in Equation 6 is a weighting factor that is a function of the depth (z) in meters.

$$F = \begin{cases} 1 - FS & \text{If FS} < 1 \\ 0 & \text{Otherwise} \end{cases} \tag{5}$$

$$w(z) = 10 - 0.5.Z \tag{6}$$

The LPI is calculated for more than 1000 CPT soundings available in the area of interest (Figure 16) and a spatial map of the LPI is then generated using bilinear interpolation. Figure 16 compares the GGLM-predicted LSE and CPT-based generated LPI maps as well as the spatial map of the property-by-property field observation of liquefaction (NZGD, 2013). The LSE has been plotted as four categories to best parallel the LPI categories proposed by Iwasaki et. al (1978) as presented in Table 5.

Table 5. Classification of the LPI (Iwasaki et al., 1978)

LPI value	Liquefaction severity
0-5	1-No liquefaction
5-10	2-marginal
10-15	3-Moderate
>15	4-Severe

As can be seen in Figure 16, the LPI values are more variable across the study area which is linked with the variation in geotechnical aspects of soil profile across the study area. Reversely, the spatial distribution of LSE values seems to be more clustered and more linked with regional properties which is consistent with the geospatial explanatory variables. Considering that the LSE map is generated using globally available geospatial proxies while the LPI map is generated from hundreds of CPT soundings, the performance of the GGLM seems to be fairly good and acceptable even in a local scale comparing to the LPI map. Both spatially-generated LPI and LSE maps mismatch the property-by-property observation of liquefaction in some parts of the affected area.

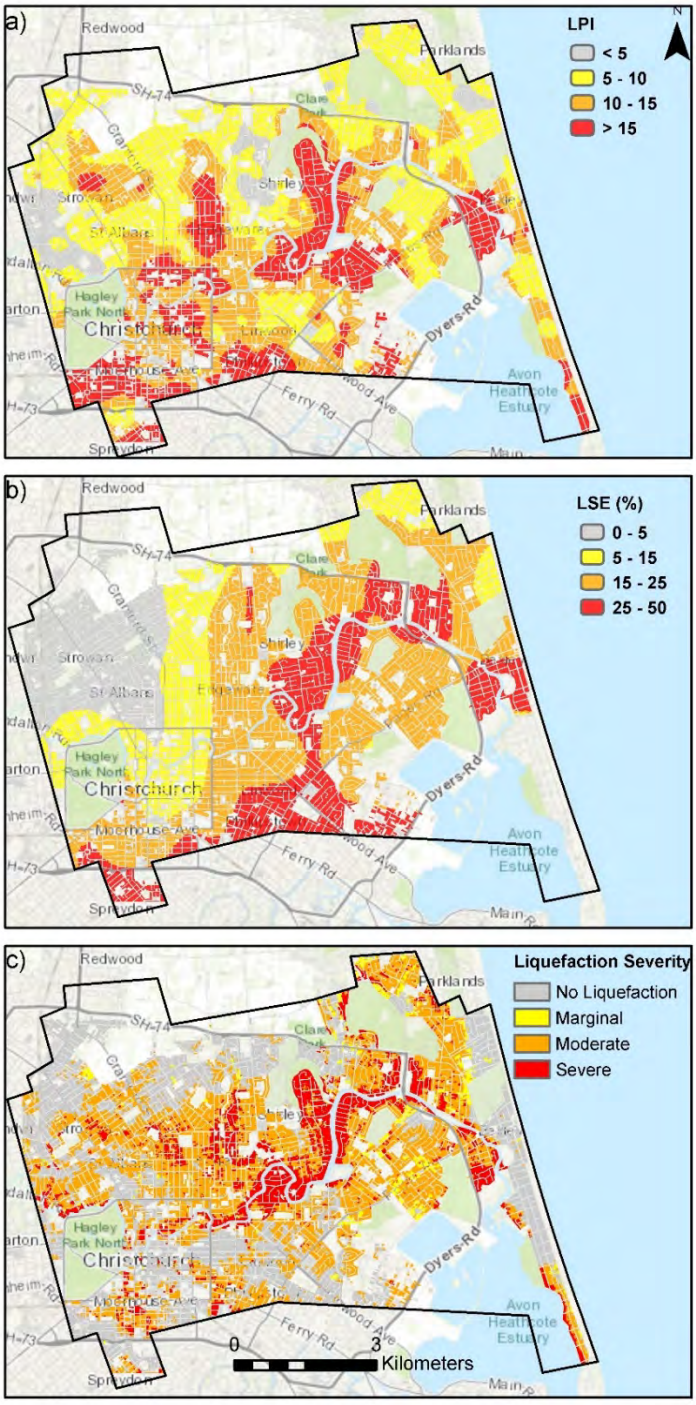

Figure 16. Comparison between field observation of liquefaction severity, local LPI and global LSE maps

5. Conclusion

The Global Geospatial Liquefaction Model (GGLM) proposed by Zhu et. al (2017) is evaluated for 53 coastal and non-coastal earthquake events across the globe and in six different regions. The GGLM was modified herein to include a PGA threshold of 0.1g in addition to the original PGV threshold of 3 cm/s. In all events in which liquefaction was observed, the model was able to capture the majority of the liquefaction points observed by the reconnaissance team. Also in most of the events that liquefaction was not observed, the GGLM predicted no to minor liquefaction extent; the only exception is the 2008 Iwate earthquake in Japan in which no liquefaction was observed (but lateral spreading was observed) while the model predicted large liquefaction spatial extent. The liquefaction spatial extent (LSE) was summed for each earthquake and called as LSE intensity score. The LSE intensity score was compared with the liquefaction intensity inferred from the field observation and classified into four liquefaction intensity categories for easy reporting and integration into rapid response systems such as PAGER. Overall, the GGLM performance was appropriate for regional evaluation of post-event liquefaction. Overprediction of liquefaction was observed in India, Nepal, and Central America. The performance of GGLM as a global predictor was investigated at urban scale by comparing LSE and LPI spatial map in the Christchurch area. The result demonstrated the acceptable performance of the GGLM as compared to the LPI for predicting the severity of liquefaction even at the regional scale.

6. Reference

Bardet, J. P., Deaton, S., Frost, D., Goel, P., Lettis, W., Moss, R., & Stewart, J. (2001). Initial geotechnical observations of the Bhuj, India, Earthquake of January 26, 2001. *Geotechnical Extreme Events Reconnaissance (GEER) Association*.

Bhattacharya, S., Hyodo, M., Goda, K., Tazoh, T., & Taylor, C. A. (2011). Liquefaction of soil in the Tokyo Bay area from the 2011 Tohoku (Japan) earthquake. *Soil Dynamics and Earthquake Engineering*, *31*(11), 1618-1628.

Bray, J. D., Sancio, R., Kammerer, A. M., Merry, S., Rodriguez-Marek, A., Khazai, B., & Dreger, D. (2001). Some Observations of the Geotechnical Aspects of the February 28, 2001, Nisqually Earthquake in Olympia, South Seattle, and Tacoma, Washington. *Report sponsored by NSF, PEER Center, UCB, University of Arizona, Washington State University, Shannon and Wilson Inc., and Leighton and Associates*.

Bray, J., Cohen-Waeber, J., Dawson, T., Kishida, T., & Sitar, N. (2014). Geotechnical engineering reconnaissance of the August 24, 2014 M6 South Napa earthquake. *Geotechnical Extreme Events Reconnaissance (GEER) Association. doi*, *10*(2.1), 1094-7844.

Candia, G., de Pascale, G., Montalva, G., & Ledezma, C. Geotechnical Reconnaissance of the 2015 Illapel Earthquake. *Geotechnical Extreme Events Reconnaissance (GEER) Association.*

Carter, M., & Maurer, B. (2011). Geotechnical Quick Report on the Affected Region of the 23 August 2011 M5. 8 Central Virginia Earthquake near Mineral, Virginia. *Geotechnical Extreme Events Reconnaissance (GEER) Association*

Chleborad, A. F., & Schuster, R. L. (1990). *Ground failure associated with the Puget Sound region earthquakes of April 13, 1949, and April 29, 1965* (No. 90-687). US Geological Survey.

Clayton, P., Zalachoris, G., Rathje, E., Bheemasetti, T., Caballero, S., Yu, X., & Bennett, S. (2016). The Geotechnical Aspects of the September 3, 2016 M 5.8 Pawnee, Oklahoma Earthquake. *Geotechnical Extreme Events Reconnaissance (GEER) Association. doi*, *10*, G69885.

Cubrinovski, M., Green, R. A., Wotherspoon, L., Allen, J., Bradley, B., Bradshaw, A., & Pender, M. (2011). Geotechnical reconnaissance of the 2011 Christchurch, New Zealand earthquake. *Geotechnical Extreme Events Reconnaissance (GEER) Association*.

Cubrinovski, M., Green, R., Allen, J., Ashford, S., Bowman, E., Bradley, B.A., & Cox, B. (2010). Geotechnical reconnaissance of the 2010 Darfield (New Zealand) earthquake. *Geotechnical Extreme Events Reconnaissance (GEER) Association*.

Erdik, M., Kamer, Y., Demircioğlu, M., & Şeşetyan, K. (2012). 23 October 2011 Van (Turkey) earthquake. *Natural hazards*, *64*(1), 651-665.

Fan, Y., Li, H., & Miguez-Macho, G. (2013). Global patterns of groundwater table depth. *Science*, *339*(6122), 940-943.

Gómez, J. C., Tavera, H. J., & Orihuela, N. (2005). Soil liquefaction during the Arequipa Mw 8.4, June 23, 2001 earthquake, southern coastal Peru. *Engineering Geology*, *78*(3), 237-255.

Goto, K., Sugawara, D., Abe, T., Haraguchi, T., & Fujino, S. (2012). Liquefaction as an important source of the AD 2011 Tohoku-oki tsunami deposits at Sendai Plain, Japan. *Geology*, *40*(10), 887-890.

Hamada, M., Isoyama, R., & Wakamatsu, K. (1996). Liquefaction-induced ground displacement and its related damage to lifeline facilities. *Soils and foundations*, *36*(Special), 81-97.

Hashash, Y., Tiwari, B., Moss, R. E., Asimaki, D., Clahan, K. B., Kieffer, D. S., & Pehlivan, M. (2015). Geotechnical field reconnaissance: Gorkha (Nepal) earthquake of April 25, 2015 and related shaking sequence. *Geotechnical Extreme Events Reconnaissance (GEER) Association*.

Holzer, T. L. (Ed.). (1998). *The Loma Prieta, California, earthquake of October 17, 1989* (Vol. 1550). Government Printing Office.

Holzer, T. L., Noce, T. E., Bennett, M. J., Tinsley III, J. C., & Rosenberg, L. I. (2005). Liquefaction at Oceano, California, during the 2003 San Simeon earthquake. *Bulletin of the Seismological Society of America*, *95*(6), 2396-2411.

Huang, Y., & Jiang, X. (2010). Field-observed phenomena of seismic liquefaction and subsidence during the 2008 Wenchuan earthquake in China. *Natural Hazards*, *54*(3), 839-850.

ISHIHARA, K., & KOGA, Y. (1981). Case studies of liquefaction in the 1964 Niigata earthquake. *Soils and foundations*, *21*(3), 35-52.

Iwasaki, T. (1978). A practical method for assessing soil liquefaction potential based on case studies at various sites in Japan. In *Proc. Second Int. Conf. Microzonation Safer Construction Research Application, 1978* (Vol. 2, pp. 885-896).

Kayen, R., Brandenberg, S. J., Collins, B. D., Dickenson, S., Ashford, S., Kawamata, Y., & Tokimatsu, K. (2009). Geoengineering and seismological aspects of the Niigata-Ken Chuetsu-Oki earthquake of 16 July 2007. *Earthquake Spectra*, *25*(4), 777-802.

Kayen, R., Cox, B., Johansson, J., Steele, C., Somerville, P., Konagai, K., Zhao, Y., Tanaka, H. (2008). Geoengineering and Seismological Aspects of the Iwate Miyagi-Nairiku, Japan

Earthquake of June 14, 2008. . *Geotechnical Extreme Events Reconnaissance (GEER) Association*.

Kayen, R., Thompson, E., Minasian, D., Moss, R. E., Collins, B. D., Sitar, N., ... & Carver, G. (2004). Geotechnical reconnaissance of the 2002 Denali fault, Alaska, earthquake. *Earthquake Spectra*, *20*(3), 639-667.

Kiyono, J., Fujiwara, T., Hamada, M., Hashimoto, T., Ichii, K., Isoyama, R., & Nozaki, T. (2007). Reconnaissance report on the 2000 Tottori-ken Seibu Earthquake. *Doboku Gakkai Ronbunshuu A*, *63*(2), 374-385.

Luna, R. (2010). Reconnaissance Report of the May 28, 2009 Honduras Earthquake, M 7.3. *Geotechnical Extreme Events Reconnaissance (GEER) Association*.

Miura, S., Yagi, K., & Kawamura, S. (1995). Liquefaction damage of sandy and volcanic grounds in the 1993 Hokkaido Nansei-Oki earthquake.

Monaco, P., De Magistris, F. S., Grasso, S., Marchetti, S., Maugeri, M., & Totani, G. (2011). Analysis of the liquefaction phenomena in the village of Vittorito (L'Aquila). *Bulletin of Earthquake Engineering*, *9*(1), 231-261.

Mukunoki, T., Kasama, K., Murakami, S., Ikemi, H., Ishikura, R., Fujikawa, T., & Kitazono, Y. (2016). Reconnaissance report on geotechnical damage caused by an earthquake with JMA seismic intensity 7 twice in 28h, Kumamoto, Japan. *Soils and Foundations*, *56*(6), 947-964.

New Zealand Geotechnical Database, NZGDs (2013). "Liquefaction and Lateral Spreading Observations", *Map Layer CGD0300 - 11 Feb 2013*, retrieved from

Nikolaou, S., Vera-Grunauer, X., Gilsanz, R., Luque, R., Kishida, T., Diaz-Fanas, G., & Alzamora, D. (2016). GEER-ATC M 7.8 April 16, 2016 Muisne, Ecuador earthquake reconnaissance report. *Geotechnical Extreme Events Reconnaissance (GEER) Association.*

Olson, S. M., Green, R. A., Lasley, S., Martin, N., Cox, B. R., Rathje, E., & French, J. (2011). Documenting liquefaction and lateral spreading triggered by the 12 January 2010 Haiti earthquake. *Earthquake Spectra*, *27*(S1), S93-S116.

Papathanassiou, G., Caputo, R., & Rapti-Caputo, D. (2012). Liquefaction phenomena along the paleo-Reno River caused by the May 20, 2012, Emilia (northern Italy) earthquake. *Annals of Geophysics*, *55*(4).

Papathanassiou, G., Ganas, A., & Valkaniotis, S. (2016). Recurrent liquefaction-induced failures triggered by 2014 Cephalonia, Greece earthquakes: Spatial distribution and quantitative analysis of liquefaction potential. *Engineering Geology*, *200*, 18-30.

Pavlides, S., Papathanassiou, G., Valkaniotis, S., Chatzipetros, A., Sboras, S., & Caputo, R. (2013). Rock-falls and liquefaction related phenomena triggered by the June 8, 2008, M. *Annals of Geophysics*, *56*(6), S0682.

Rathje, E. M., Karatas, I., Wright, S. G., & Bachhuber, J. (2004). Coastal failures during the 1999 Kocaeli earthquake in Turkey. *Soil Dynamics and Earthquake Engineering*, *24*(9), 699-712.

Rathje, E. M., Kelson, K., Ashford, S. A., Kawamata, Y., Towhata, I., Kokusho, T., & Bardet, J. P. (2006). Geotechnical Aspects of the 2004 Niigata Ken Chuetsu, Japan, Earthquake. *Earthquake Spectra*, *22*(S1), 23-46.

Rollins, K., Franke, K., Luna, B. R., Rocco, N., Avila, D., Climent , M. R. (2013). Geotechnical aspects of sept. 5, 2012 m7.6 Samara, Costa rica earthquake. *Geotechnical Extreme Events Reconnaissance (GEER) Association*.

Rollins, K., Ledezma, C., & Montalva, G. (2014). Geotechnical aspects of April 1, 2014, M8. 2 Iquique, Chile Earthquake. *Geotechnical Extreme Events Reconnaissance (GEER) Association*.

Stewart, J. P., & Brandenberg, S. J. (2010). Preliminary report on seismological and geotechnical engineering aspects of the April 4 2010 mw 7.2 El Mayor-Cucapah (Mexico) earthquake. *Geotechnical Extreme Events Reconnaissance (GEER) Association*

Stewart, J. P., Bray, J. D., Seed, R. B., & Sitar, N. (1994). Preliminary report on the principal geotechnical aspects of the January 17, 1994 Northridge earthquake. *University of California, Berkeley, Earthquake Engineering Research Center] Report UCB/EERC-94/08. Berkeley: Earthquake Engineering Research Center, University of California*.

Sucuoğlu, H. (2000). The 1999 Kocaeli and Düzce-Turkey Earthquakes. *Middle East Technical University*.

Sun, J., Hutchinson, T., Clahan, K., Menq, F., Lo, E., Chang, W. J., & Ma, K. F. (2016). Geotechnical reconnaissance of the 2016 Mw6. 3 Meinong Earthquake, Taiwan. *Geotechnical Extreme Events Reconnaissance (GEER) Association*.

Taucer, F., Alarcon, J. E., & So, E. (2009). 2007 August 15 magnitude 7.9 earthquake near the coast of Central Peru: analysis and field mission report. *Bulletin of Earthquake Engineering*, *7*(1), 1-70.

Thompson, E.M. (2017). Personal Communication.

Tohno, I., & shamoto, Y. (1985). Liquefaction Damage to the Ground during the 1983 Nihonkai-Chubu (Japan Sea) Earthquake in Akita Prefecture, Tohoku, Japan. *Natural disaster science*, *7*(2), 67-93.

Tohno, I., & Yasuda, S. (1981). Liquefaction of the ground during the 1978 Miyagiken-Oki earthquake. *Soils and Foundations*, *21*(3), 18-34.

Verdugo, R. (2011). Comparing liquefaction phenomena observed during the 2010 Maule, Chile earthquake and 2011 Great East Japan earthquake. In *Proceedings of international symposium on engineering lessons learned from the* (pp. 1-4).

Wakamatsu, K. (2011). Historic Liquefaction sites in Japan, 745-2008, University of Tokyo Press.

Wald, D. J., Jaiswal, K., Marano, K. D., Bausch, D., & Hearne, M. (2010). *PAGER--Rapid assessment of an earthquake's impact*. United States Geological Survey.

Wald, D. J., & Allen, T. I. (2007). Topographic slope as a proxy for seismic site conditions and amplification. *Bulletin of the Seismological Society of America*, *97*(5), 1379-1395.

Wartman, J., Rodriguez-Marek, A., Macari, E. J., Deaton, S., Ramírez-Reynaga, M., Ochoa, C. N., & Ovando-Shelley, E. (2005). Geotechnical aspects of the January 2003 Tecoman, Mexico, earthquake. *Earthquake spectra*, *21*(2), 493-538.

Worden, C. B., Wald, D. J., Allen, T. I., Lin, K., Garcia, D., & Cua, G. (2010). A revised ground-motion and intensity interpolation scheme for ShakeMap. *Bulletin of the Seismological Society of America*, *100*(6), 3083-3096.

Yasuda, S., Watanabe, H., Yoshida, N., & Mora, S. (1993). Soil Liquefaction During the 1991 Telire-Limón, Costa Rica, Earthquake.

Yuan, H., Yang, S. H., Andrus, R. D., & Juang, C. H. (2004). Liquefaction-induced ground failure: a study of the Chi-Chi earthquake cases. *Engineering Geology*, *71*(1), 141-155.

Zhu, J., Baise, L. G., & Thompson, E. M. (2017). An Updated Geospatial Liquefaction Model for Global Application. *Bulletin of the Seismological Society of America*, *107*(3), 1365-1385.

Zhu, J., Daley, D., Baise, L. G., Thompson, E. M., Wald, D. J., & Knudsen, K. L. (2015). A geospatial liquefaction model for rapid response and loss estimation. *Earthquake Spectra*, *31*(3), 1813-1837.

Zimmaro, P., & Stewart, J. P. (2016). Engineering reconnaissance following the 2016 M 6.0 Central Italy Earthquake. *Geotechnical Extreme Events Reconnaissance (GEER) Association*.